AD-A284 874

PROJECT

"SYNTHESIS AND APPLICATIONS

OF LARGE HETEROMETALLIC CLUSTER SYSTEMS"

CONTRACT NO: DA3A45-90-C-0034

Seventh Interim Report

October 1993

94 9 23 077

Best Available Copy

ULTRAFAST NONLINEARITY OF

GOLD NANOPARTICLES

Kathleen Puech
Trinity College Dublin

1.   **Summary of Progress**

        Work has proceeded according to schedule on all research topics.

(i)   Uniquely well defined clusters of Gold are now available for optical measurements.

(ii)   A comprehensive experimental investigation has been carried out to determine the non-linearity of these samples on a femtosecond timescale. These results are presented below and prove that:

>   (a)   the nonlinear refractive index rises and relaxes on a sub-picosecond timescale.

>   (b)   the nonlinearity is predominant positive imaginary originating from a hot electron contribution.

>   (c)   the nonlinearity is <u>independent</u> of the size of the particle.

2.   **Staffing**

        No major changes in staffing have taken place.

CHAPTER 1

INTRODUCTION

The interaction of light with matter is usually characterised by several phenomena, such as light absorption, refraction, scattering etc. All of these are regarded as linear optical properties of the material, dependent on wavelength but independent of the intensity of the light. However, if the illumination is made sufficiently intense, the optical properties begin to depend on the intensity and other characteristics of the light. The light waves may then interact with each other as well as with the medium. The study of such interactions is the field of nonlinear optics. It is a field that has experienced a rapid growth of interest. There are three main motivations for this. First, there is the possibility of exploiting the nonlinear behaviour in various devices. The most important of these are frequency converters, in which laser radiation at one frequency is converted into coherent radiation at a new frequency, by, for example, harmonic generation, sum-frequency generation etc.[1] Because the converted radiation may be at a frequency that is not directly available from a laser source, these frequency conversion techniques provide an important means of extending the spectral range covered by coherent sources. A second reason for studying nonlinear optical processes is that they set a limit to the light flux that can be passed through a medium. For example, two photon absorption can lead to depletion of the incident light and self-focusing leads to distortion of the incident beam profile. A third interest in nonlinear optical effects lies in their use as a means of obtaining information about the microscopic properties of the atoms of molecules that constitute the nonliner medium. . Two photon absorption, for example, can be used to study energy levels that are inaccessible by single photon absorption.

When an electric field is incident on a conductor consisting of negatively and positively charged particles, it gives rise to a flow of current - the positive charges move in the direction of the field while the negative ones move in the opposite direction. In the case of dielectric's, on the other hand, the charged particles are not free to move but are bound together. The effect of an electric field on such materials is to induce a polarisation that is proportional to the applied field. However, as the intensity of the field is increased the linear dependence of the two terms no longer holds. The polarisation must now be expressed as a power series in the field, as follows :

$$P = \varepsilon_0(\chi^{(1)}E + \chi^{(2)}E^2 + \chi^{(3)}E^3 + ...)$$

(1.1)

1

Where, χ = Linear susceptibility, and

$\chi^{(2)}$, $\chi^{(3)}$, ... = Nonlinear susceptibilities.

The nonlinear susceptibility is a tensor object and reflects the symmetry of the material. For a crystal with inversion symmetry, i.e. one that is centrosymmetric, the second term and higher even terms, $\chi^{(2)}$, $\chi^{(4)}$ etc., are zero. However $\chi^{(3)}$ is always non zero.

At first crystalline nonlinear media were seen to offer the greatest device potential. The reason for this lay in the fact that $\chi^{(2)}$ is zero unless the medium lacks a centre of symmetry. Nonlinear effects in centrosymmetric media would thus depend on higher-order and therefore presumably smaller nonlinear terms. Unfortunately, however, few crystalline materials have proved capable of satisfying the list of requirements for a good nonlinear material. A number of significant advantages are offered by liquids and gases. They can be easily prepared, with good optical quality over large dimensions. Also, they are less prone to suffer irreversible damage at high intensities.

In order for nonlinear behaviour to manifest itself, the field incident on the material must be comparable to the internal field E_a which binds together its electrons and ions; typically $E_a \approx 3 \times 10^{10} Vm^{-1}$. To obtain an optical field of such a magnitude, an incident intensity of $\approx 10^{14} Wcm^{-2}$ is required. However, such high intensities are not in fact necessary for the observation of many nonlinear-optical effects. One reason is that, provided the assembly of induced dipoles oscillates coherently, the field that they radiate individually can, in certain circumstances, add together constructively to produce a much larger total intensity. This phenomenon is termed "phase matching".

The intensity required to observe some nonlinear processes can be further reduced by many orders of magnitude by choosing one or more of the optical frequencies involved so that they lie close to a resonant frequency of the oscillating dipoles; this is termed "resonance enhancement". In nonlinear optics resonant enhancement is utilised in two ways : Firstly, it allows nonlinear processes and devices to operate effectively at lower power levels, thus increasing their range of use and efficiency. Secondly, resonant nonlinear phenomena provide the basis for "nonlinear spectroscopy"; the observation of these effect can provide information about the structure of matter that is not accessible using conventional linear optical spectroscopy.

In order to be useful in an optoelectronic device, a material requires a large nonlinear susceptibility along with a fast response time. The aim of this study is to

determine what properties of a material come into play in the enhancement of these parameters.

THE SUSCEPTIBILITY TENSOR

By considering the dynamic behaviour of charged particles in a medium under the influence of an electric field, it is possible to derive explicit formulae for the susceptibility tensors of the medium. For simplicity it is assumed that the medium consists of an assembly of microscopic polarizable units which are independent and non interacting. Thus local field factors are neglected. Local field corrections can be introduced later without altering the general formula.

A straightforward derivation, using the density matrix approach leads to the following formula for the third order susceptibility tensor $\chi^{(3)}$, that depends on the frequencies ω_1, ω_2, and ω_3 of the three electric fields involved

$$\chi_{\mu\alpha\beta\gamma}^{(3)}\left(-\omega_\sigma,\omega_1,\omega_2,\omega_3\right) = \frac{Ne^4}{\varepsilon_0 3! \hbar^3} S \sum_{abcd} \rho_0(a) \ x$$

$$\left\{ \frac{r_{ab}^\mu r_{bc}^\alpha r_{cd}^\beta r_{da}^\gamma}{\left(\Omega_{ba}-\omega_1-\omega_2-\omega_3\right)\left(\Omega_{ca}-\omega_2-\omega_3\right)\left(\Omega_{da}-\omega_3\right)} + \right.$$

$$\frac{r_{ab}^\alpha r_{bc}^\mu r_{cd}^\beta r_{da}^\gamma}{\left(\Omega_{ba}+\omega_1\right)\left(\Omega_{ca}-\omega_1-\omega_2\right)\left(\Omega_{da}-\omega_3\right)} + \frac{r_{ab}^\alpha r_{bc}^\beta r_{cd}^\mu r_{da}^\gamma}{\left(\Omega_{ba}+\omega_1\right)\left(\Omega_{ca}+\omega_1+\omega_2\right)\left(\Omega_{da}-\omega_3\right)}$$

$$\left. + \frac{r_{ab}^\alpha r_{bc}^\beta r_{cd}^\gamma r_{da}^\mu}{\left(\Omega_{ba}+\omega_1\right)\left(\Omega_{ca}+\omega_1+\omega_2\right)\left(\Omega_{da}+\omega_1+\omega_2+\omega_3\right)} \right\} \qquad (1.2)$$

Where μ, α, β, γ are summed over the co-ordinates x, y and z,

$\omega_\sigma = \omega_1 + \omega_2 + \omega_3$, where ω_1, ω_2, and ω_3 are the frequencies of the applied fields,

the operator S implies intrinsic permutation symmetry,

N is the number density of molecules, i.e. the number of molecules/unit volume,

er_{ab}^μ is the (ab)th element of the dipole moment matrix er^μ, and

$\Omega_{ba} = \dfrac{E_b - E_a}{\hbar}$ is the transition frequency.

3

This expression has singularities in the frequency domain whenever any one of the frequency denominators of the type $\Omega - \omega$ approaches zero. Thus the susceptibility may be "resonantly enhanced" by choosing one or more of the incident frequencies, or combinations of them, to coincide with an optical transition frequency of the medium. Obviously, as is apparent from the above formula, for the largest nonlinear susceptibilities we require large values for the matrix elements of the electric-dipole operator $e\mathbf{r}$ and small frequency denominators.

The use of resonance's to enhance a specific susceptibility often has the effect of similarly enhancing other competing or undesirable processes. For example, by allowing an input frequency to approach resonance with a single-photon molecular transition, that input field may suffer a corresponding increase in absorption; this occurs because the first-order susceptibility $\chi^{(1)}$ is also enhanced.

For very close resonance, the mathematical divergence's in the above formula are unphysical; they occur only because higher order nonlinearities have been neglected. When excited very close to resonant transitions, the molecules undergo large perturbations - thus invalidating the small-perturbation approximations - and the transition frequencies which occur in the denominator terms become field-dependent themselves. When these strong field dependent perturbations, or level shifts, are taken into account, the resulting induced polarisation remains finite. In many cases, however, the resonant nonlinearities are dominated by various transition-line broadening processes, perhaps due to interactions between the molecules, which also ensure that the resonant susceptibilities do not diverge. A particular resonant process can then be represented by a single order of nonlinearity derived using the small-perturbation analysis, but with the addition of appropriate damping terms $\pm i\Gamma$ in the frequency denominators of the susceptibilities as for example $\left(\Omega_{ba} + i\Gamma_{ba} - \omega_\sigma\right)$. The damping factor Γ_{ba} is thus identified as a dephasing parameter appropriate to weak collisions, and as such represents a spectral linewidth for the transition of frequency Ω_{ba}. The smallest values which the damping factors Γ can take are determined by spontaneous emission, and in this case Γ_{ba}^{-1} is a natural lifetime in the absence of collisions and other perturbations.

Thus when damping terms are inserted into the expression for the general third-order susceptibility, the following expression is obtained :

$$\chi^{(3)}_{\alpha\beta\gamma}\left(-\omega_\sigma,\omega_1,\omega_2,\omega_1\right) = \frac{Ne^4}{\varepsilon_0 3!\hbar^3} S \sum_{abcd} \rho_0(a)$$

$$\left\{ \frac{\mathbf{e}_\sigma.\mathbf{r}^\mu_{ab}\mathbf{e}_1.\mathbf{r}^\alpha_{bc}\mathbf{e}_2.\mathbf{r}^\beta_{cd}\mathbf{e}_1.\mathbf{r}^\gamma_{da}}{\left(\Omega_{ba}-i\Gamma_{ba}-\omega_\sigma\right)\left(\Omega_{ca}-i\Gamma_{ca}-\omega_2-\omega_1\right)\left(\Omega_{da}-i\Gamma_{da}-\omega_1\right)} + \right.$$

$$\frac{\mathbf{e}_1.\mathbf{r}^\alpha_{ab}\mathbf{e}_\sigma.\mathbf{r}^\mu_{bc}\mathbf{e}_2.\mathbf{r}^\beta_{cd}\mathbf{e}_1.\mathbf{r}^\gamma_{da}}{\left(\Omega_{ba}+i\Gamma_{ba}+\omega_1\right)\left(\Omega_{ca}-i\Gamma_{ca}-\omega_2-\omega_1\right)\left(\Omega_{da}-i\Gamma_{da}-\omega_1\right)} +$$

$$\frac{\mathbf{e}_1.\mathbf{r}^\alpha_{ab}\mathbf{e}_2.\mathbf{r}^\beta_{bc}\mathbf{e}_\sigma.\mathbf{r}^\mu_{cd}\mathbf{e}_1.\mathbf{r}^\gamma_{da}}{\left(\Omega_{ba}+i\Gamma_{ba}+\omega_1\right)\left(\Omega_{ca}+i\Gamma_{ca}+\omega_1+\omega_2\right)\left(\Omega_{da}-i\Gamma_{da}-\omega_1\right)} +$$

$$\left. \frac{\mathbf{e}_1.\mathbf{r}^\alpha_{ab}\mathbf{e}_2.\mathbf{r}^\beta_{bc}\mathbf{e}_1.\mathbf{r}^\gamma_{cd}\mathbf{e}_\sigma.\mathbf{r}^\mu_{da}}{\left(\Omega_{ba}+i\Gamma_{ba}+\omega_1\right)\left(\Omega_{ca}+i\Gamma_{ca}+\omega_1+\omega_2\right)\left(\Omega_{da}+i\Gamma_{da}+\omega_\sigma\right)} \right\} \tag{1.4}$$

Clearly, if the frequency which appears in a particular denominator term is far removed from molecular resonance's, then the corresponding damping term can be safely neglected.

A price paid for the resonant enhancement of optical nonlinearity is the slowing-down of the speed of response, which may be a serious limitation for some applications such as optical switching and signal processing.

The work done for this thesis is based on the measurement of the resonantly enhanced nonlinear susceptibility, $\chi^{(3)}$ of colloidal gold solutions, with the diameters of the gold particles varying from 50-400Å. The reason for interest in these materials lies in the fact that the properties of the inclusions are completely different from bulk gold because of their small dimensions. This results in two confinement effects, quantum confinement and dielectric confinement, which both have potential in enhancing the macroscopic susceptibility of the solution and are also in themselves very interesting phenomena to study. In chapter 2 the materials are described in more detail and the confinement effects mentioned here are elaborated upon. Chapters 3, 4, 5 and 6 describe different experimental techniques that were used to study the materials and in particular to measure their susceptibility and response times. Chapter 7 gives the final conclusions of this study based on, both, the results obtained here *and* findings in the extensive literature on this topic.

REFERENCES

1.1   Franken, P. A., Hill, A. E., Peters, C. W. and Weinreich, G. (1961) Phys. Rev. Lett. 7, 118

CHAPTER 2

THE OPTICAL PROPERTIES OF ARTIFICIAL MATERIALS

In the early days of nonlinear optics, the materials used for experiments and devices were mainly inorganic dielectric crystals, vapours, liquids and bulk semiconductors. More recently, interest has been focused on new artificial solid state materials which offer higher nonlinearity, and in particular, those that allow nonlinear optical devices to operate efficiently at relatively low power levels. Several materials with large second-order nonlinearity have been successfully fabricated [1]. These have applications in devices such as compact optical-frequency doublers and parametric amplifiers and oscillators. However, materials with large *third*-order nonlinearity are of greater interest currently, since the nonlinear refractive-index effect can be exploited for switching, optical bistability, phase conjugation and other types of signal processing [2]. A lot of advances have been made, of late, in the synthesis of organic materials, inorganic semiconductors and metallic clusters and particles with a large third order nonlinearity. The emphasis of this study is on composite materials composed of small metallic particles embedded in a dielectric matrix. A composite medium is made of (at least) two different component media, but it is not an alloy as they are not mixed at the atomic level.

The linear optical properties of metal colloids, consisting of metal particles suspended in a dielectric matrix have been studied for a long time [3, 4]. The first models aiming at describing these properties were developed at the turn of the century [5, 6]. However, it was not until the 1980's that these materials were studies as nonlinear optical materials [7, 8]. Subsequently a lot of work has gone into investigating them. The discovery that they exhibit a relatively large band-edge resonant third-order nonlinearity with relaxation times as short as 5ps has stimulated much of the current investigation [9, 10, 11, 12, 13]. The linear dimensions of the conducting particles in these composite materials are of the order of a few nanometers and the carriers in them are confined in all three directions. It is therefore customary to refer to them as quantum dots or zero dimensional structures [14]. This term is appropriate only when the dimensions of the confinement are smaller than the mean free path of the carriers. Then the description of the optical behaviour involves the energy eigenvalues and eigenfunctions resulting from the carrier confinement.

2.1 MATERIAL PREPARATION

The materials used in this study consisted of colloidal suspensions of different sized gold particles in deionised water. The diameters of the gold particles ranged from 50-400A. The sols are labelled C(50A), K(172A), M(392A), N(395A), O(365A), P(52Å), Q(47Å), R(326Å), Y(179Å), Z(164Å) and S(184Å). Sols K, M, N, O, R, Y and Z were prepared according to the method of Frens [15] - reduction of chloroauric acid solution by Sodium citrate, which (when successful) produces possibly the most monodisperse form of divided metal known in the colloidal size regime.[16] Sols P and Q were synthesised by alkaline tetrakis (hydromethyl) phosphonium chloride reduction of chloroauric acid.[17] All the hydrosols were additionally concentrated by removal of the solvent (water) before measurement of the nonlinear optical properties. For sols P and Q, soduim citrate was added and the sols boiled for 15 minutes before concentration. For all the sols, PVP_{40k} was added, to a concentration of about 2 g/mM of metal atoms, before boiling down using a hot plate, either in a stream of nitrogen or air.

All the chemicals used were analytical reagent grade, except tetrakis (hydromethyl) phosphonium chloride which was only a general purpose reagent (Fluka). Chloroauric acid was used as obtained from Johnson Matthey and contained 49.47% metal, by weight. Poly(N-vinyl-2-pyrrolidone) at 40,000 molecular weight (PVP_{40k}) and at 10,000 (PVP_{40k}) were used, as supplied by Polysciences inc.. All water used as the dispersion medium of the sols was distilled twice, latterly from an all-glass apparatus.

2.2 MATERIAL CHARACTERISATION

The materials were characterised using Transmission Electron Microscopy (TEM), linear UV-Visible absorption spectroscopy and a range of nonlinear optical techniques. The following two subsections describe the linear characterisation methods, i.e. TEM and UV-Visible absorption spectroscopy.

2.2.1 TRANSMISSION ELECTRON MICROSCOPY :

Transmission electron microscopy is an extremely useful technique for determining the size and shape of nanometric particles and is particularly attractive in this case because of the high contrast afforded by the interface between the gold inclusions and the surrounding water. Transmission electron microscopy was performed using an Hitachi H7000 transmission electron microscope operating at 100

kV acceleration voltage. Small volumes of the concentrated sols were diluted to a metal concentration of about 1 - 2 mM with doubly distilled water and a drop of each placed for several seconds in contact with a thin non-perforated carbon film supported on a 3.05 mm copper grid. The particle profiles were measured according to their "equivalent circle diameter", and the resulting distributions of diameters assessed for their means and coefficients of variation (standard deviation of the distribution expressed as a percentage fraction of the mean). Unfortunately, there are certain errors with electron microscopy that are hard to estimate :

i) Inaccurate magnification by the microscope.

ii) Sampling error.

iii) Artefact of size introduced by imaging conditions (extent of defocus, size of objective, apertures etc.) and

iv) Measuring inaccuracies (particularly induced by estimating equivalent circle diameters of aspherical particles).

5% is a reasonable value for the error in the absolute value of <d> (average diameter) for monodisperse sols. Since most of the errors above are systematic (apart form sampling errors and inhomogeneities which can be partially estimated by examining different micrographs and are less for monodisperse sols), comparisons between one sol and another still hold. For polydisperse sols the absolute error is greater.

Figures 2.1 a-c show typical micrographs obtained. As is evident, the size distribution of the particles is very narrow and they can be considered to be spherical to a high degree of accuracy. Micrographs taken of the same samples over a year later showed that they were free of aggregates and had the same characteristics as the freshly prepared sols.

2.2.2 UV-VISIBLE ABSORPTION SPECTROSCOPY :

UV-Visible absorption spectroscopy is a standard technique for obtaining the energies of interband, intraband and other transitions in materials. Literally 100's of papers have been published on the linear optical properties of small metal particles. See, for example references 3 and 4. The following section discusses, therefore, only briefly the general features of the linear absorbance spectrum of colloidal gold.

Electric dipole absorption in Gold composite materials results in a peak in the visible part of the absorption spectrum, called the "surface plasmon resonance" peak.

The absorption is due to a collective electron plasma oscillation (plasmon) that is coupled to an external transverse electromagnetic field through the particle surface.[18] The plasmon consists of the conduction electrons of the metal and can be classically described as a spherically bounded free electron wave that is damped. The UV light absorbed by Silver and Gold particles, on the other hand, is due to interband transitions, and is quite distinct from intraband excitation of the plasmon resonance in the visible. The fact that this free electron part of the optical response is distinct from the bound electron and/or interband contribution and occurs in the visible, is why these colloids exhibit such strong colours.

Depending upon the size of the inclusions, two different theories are used to explain the linear absorption spectra of the composite materials. The first of the two, the quasi-static or dipole approximation approach is valid when the size of the particle is much smaller than the wavelength of light incident on it. This reduces the problem to that of a particles immersed in a uniform, but time dependent, field. Thus retardation can be neglected, and only dipole modes need to be considered. The quasi-static approximation is reasonable for particles with dimensions $< 30nm$ for $\lambda = 530nm$.

Within this approximation, features of the absorption spectrum, such as position and width of the surface plasmon peak are size independent. There is, however, a theory that the *dielectric function* of a small metal sphere is dependent upon its size. This function is based on a classical model of a reduced electron mean free path or a quantum-mechanical model that leads to discrete electron energy levels. Both viewpoints predict that the imaginary part of the dielectric function will increase with decreasing particle size, leading to a broadening of the surface-plasmon width for smaller particles. The quantum mechanical model also predicts a slight blue shift in the peak position of the plasmon resonance with decreasing particle size.

When the size of the inclusions becomes larger, retardation effects have to be included. At this stage the "Mie theory" [5] is used to explain the various features of the absorption spectrum. According to the Mie theory, the plasmon resonance broadens and the peak position red shifts with increasing particle sizes - similar to the quantum mechanical predictions for small particles. The theory derives from a solution of Maxwell's equations, with boundary conditions defined such that the electric and magnetic fields just outside the sphere are the same as those just inside , i.e. the radiation must be continuous across the sphere boundaries. Using these boundary conditions, it is possible to come up with an expression relating the absorption coefficient, α, to the wavelength of the exciting radiation. It is given by,

$$\alpha = \frac{18\pi}{\lambda} p\varepsilon_i \cdot \frac{\varepsilon_i}{\left(\varepsilon_i + 2\varepsilon_h\right)^2 + 2\varepsilon_i^2} \qquad (2.1)$$

where ε_i and ε_i are the real and imaginary parts of the dielectric constant of the inclusions, p is their volume fraction and ε_h is the (purely real) dielectric constant of the host dielectric.

Figures 2.2 and 2.3 show the linear absorbance spectrum of some of the gold colloidal samples in a spectrophotometer cell of path length 1 mm.
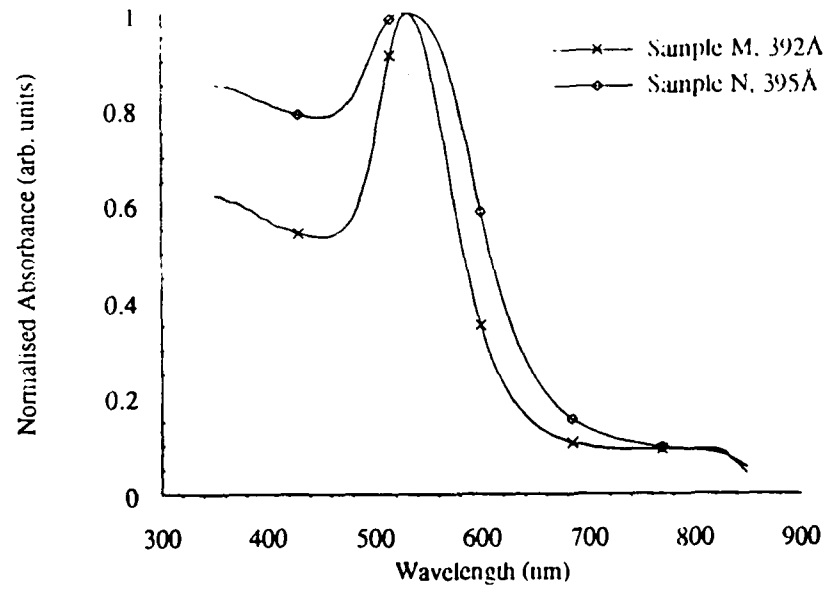

Figure 2.2 : .inear absorbance spectrum of two similarly sized gold colloids

12

Normalised Absorbance (arb. units)

1
0.8
0.6
0.4
0.2
0

—×— Sample Q. 47A
—◇— Sample S. 184A

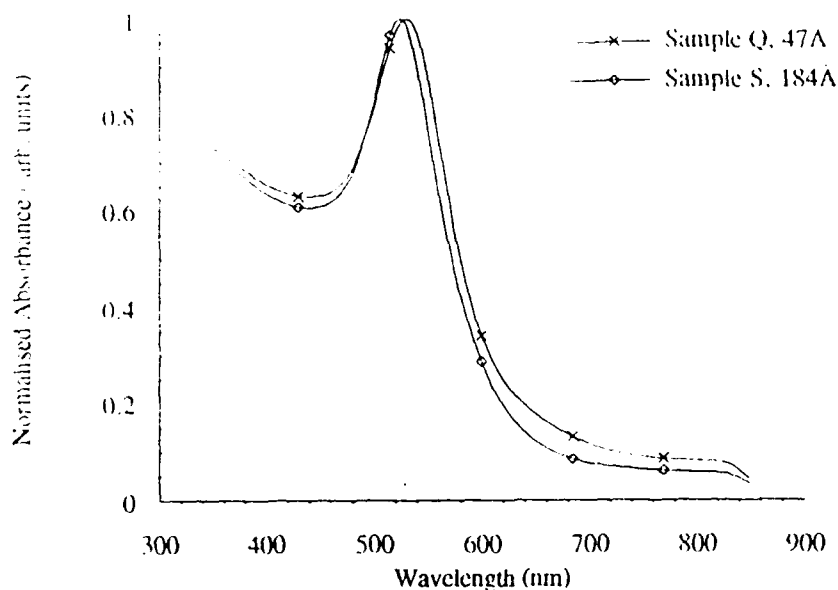300 400 500 600 700 800 900

Wavelength (nm)

Figure 2.3 : Linear absorbance spectrum of two gold colloids of completely different sizes

As is evident from the figures, it is difficult to come to any definite conclusion regarding the relationship between particle size and width of the absorption band and peak position of the plasmon resonance. It is probable that the discrepancies are at least partially due to the fact that most theoretical models are based on idealised samples i.e. an assembly of non-interacting spheres of the same size. In reality, of course, this is not the case. Unlike silver particles which have a sharp surface-plasmon resonance, the resonance in gold is broad because of the relatively large bulk value of the imaginary part of the dielectric function, ε_i^*.[19] In addition, there is the onset of an interband transition in gold near the plasmon resonance that leads to large absorption in the blue wing of the absorbance spectrum. The distribution of particle sizes and shapes,[20] the number of lattice defects [21] and the large value of the bulk dielectric constant, c, will tend to mask changes in the linear absorbance spectra that are due to a size dependent ε_i^*. The host matrix also plays an important role in determining the width and the peak position of the surface plasmon peak.

2.3 SIZE EFFECTS

Small metal particles almost never have plasmon peaks as sharp as those predicted by the simple Mie theory.[22] The reason for this is that the fundamental electronic properties of small metal particles differ from those of the bulk. i.e., small metal particles are intrinsically different from a similar volume of bulk metal, because it is the near infinite continuous lattice of metals that defines their electronic structure. This is known as the size effect.[4, 23, 24] It is an intrinsic effect, due to the change in

13

the properties of the material at small crystallite size, whereas the variation in optical properties with particle diameter (as described by the Mie theory) is an *extrinsic* effect defined by the geometry of the interaction of light with a sphere, the nature of the metal remaining unchanged.

The size effect affects the inclusions in two distinct ways. Firstly, the delocalized conduction electrons of the bulk find themselves, in the inclusions, confined to regions that are much smaller than their delocalization lengths. (For an unconfined metal, delocalization lengths extend over several unit cells). This results in discrete optical resonance's whose position, oscillator strengths and dynamics depend on the extension of the artificial confinement. This effect is known as the Quantum confinement effect (it is quantum mechanical in nature). So basically, it relates to the alternations in the energy structure of the material and comes into play when the physical dimensions of the material become comparable with the characteristic lengths that govern quantum mechanical processes.

The second effect that stems from the small size of the particles is that the electric field that acts on and polarises them is vastly different from the external macroscopic electric field applied to the composite material. This is due not only to the particle size but also because their dielectric constant is completely different from that of the surrounding matrix. This effect is known as the dielectric confinement effect.

Quantum and dielectric confinement effects will be discussed in more detail in the following two subsections. They can be used to enhance the nonlinear response of the composite material and are particularly sensitive in the optical frequency range.

2.3.1 QUANTUM CONFINEMENT :

Quantum confinement in small metal particles was discussed for the first time in a paper by Frölich published in 1937.[25] He showed that metallic matter in the form of sufficiently small grains behaves qualitatively differently from the bulk metal. The basis of his treatment of the electronic properties of these particles was the fact that the spacing between adjacent energy levels increases with decreasing particle size. He assumed that for a given particle size, the spacing between adjacent levels is constant and independent of energy. The theory is still basically unchanged except that the artificial concept of equally spaced energy levels is removed and a number of more realistic assumptions are introduced.

Metal nanocrystals occupy a position intermediate between a molecule and the bulk crystal. Therefore, the choice of a model that accounts for the coexistence of

features from both extremes is quite complex. For a system consisting of very few atoms, the most usual approach is the one using molecular orbitals, but this becomes enormously complicated as the number of atoms is increased. On the other hand, the description is greatly simplified for an infinitely extended periodic system where the behaviour of an electron can be determined by studying the appropriate Schrödinger equation which is given by

$$H\Psi(r) = \left(-\frac{h^2}{2m}\nabla^2 + V(r)\right)\Psi(r) = E\Psi(r)$$

(2.2)

where $V(r)$ is the crystal potential experienced by the electron of mass m, and $\Psi(r)$ and E are, respectively, the state function and energy of this electron.[26]

Because the ions in a perfect crystal are arranged in a regular perfect array, the potential $V(r)$ has the periodicity of the underlying Bravais lattice, i.e.

$$V(r+R) = V(r)$$

(2.3)

for all Bravais lattice vectors R.

The problem of an electron in a solid is, in principle, a many-electron problem for the full Hamiltonian of the solid contains not only the one-electron potentials describing the interactions of the electron with the atomic nuclei, but also pair potentials describing the electron-electron interactions. In the independent electron approximation these interactions are represented by an effective one-electron potential $V(r)$.

One is thus led to examine general properties of the Schrödinger equation for a single electron, i.e., equation 2.2.

Independent electrons, each of which obeys a one-electron Schrödinger equation with a periodic potential, are known as *Bloch electrons* [26] (as opposed to *free electrons* to which Bloch electrons reduce when the periodic potential is identically zero).

According to the "Bloch theorem", the eigenstates Ψ of the one-electron Hamiltonian, above, can be chosen to have the form of a plane wave times a function with the periodicity of the Bravais lattice as follows,

$$\Psi_{nk}(r) = e^{ik\cdot r}U_{nk}(r)$$

(2.4)

Where $F_n(r+R) = F_n(r)$, where R is any lattice vector. The corresponding band energy $E_n(k)$ is a reciprocal space periodic function i.e., $E_n(k+K) = E_n(k)$ where K is any reciprocal lattice vector and k is the wave vector that labels the electron state in the band n within the first Brillouin zone.

For an infinite crystal, equation 2.4 has the form of a free wave. If, however, the periodicity is broken (e.g. due to crystal boundaries or defects) then one has to represent the electron motion as a wave packet of Bloch states. If the defect encompasses several unit cells, U_n remains essentially unaffected, and close to $k = 0$ one can write,

$$\Psi' = F_n(r)U_n(r)$$ (2.5)

Where $F_n(r)$ is the envelope function that has to be solved for.

Metals are characterised by a single half-filled band up to the Fermi level E_F with electron and hole states on either side of it. The electron and hole wave functions will thus be of the form,

$$\Psi(r_e,r_h) = F(r_e,r_h)U_e(r_e,r_h)U_h(r_e,r_h)$$ (2.6)

where U_e and U_h are the cell periodic part of the Bloch band states for the conduction (electron) and valence (holes) bands respectively at $k \approx 0$. Equation 2.2 can therefore be rewritten as.

$$\left(-\frac{\hbar^2}{2m_e^*}\nabla_e^2 - \frac{\hbar^2}{2m_h^*}\nabla_h^2 + V_{eh} + V_{mb} + V_i \right)F(r_e,r_h) = EF(r_e,r_h)$$ (2.7)

Where, V_{eh} = Electron - hole coulomb interaction, V_{mb} = residual electron and hole coulomb exchange interactions, which are lumped together under the term many body effects, and V_i = Electron(hole) - impurity interaction potential.

V_{eh}, V_{mb}, and V_i collectively constitute $V(r)$. If, in addition to the above potentials, the electrons and holes find themselves confined to lengths less than their delocalization lengths, (e.g., in crystallites the motion of the charged particles is hindered by the interface with the dielectric host matrix) then an extra potential describing the confinement has to be introduced into the one-electron Hamiltonian as follows.

$$\left(-\frac{\hbar}{2m_e^*}\nabla_e^2 - \frac{\hbar}{2m_h^*}\nabla_h^2 + V_{eh} + V_{mb} + V_t + W\right)F(r_e,r_h) = EF(r_e,r_h)$$

(2.8)

The confinement potential W can be visualised as an infinite spherical potential well, i.e., $W = 0$ for $r < a$ and $W = \infty$ for $r > a$ (a is the radius of the crystallite).

The above equation can, in general, only be solved with numerical methods and even so with limited usefulness because of the uncertainties in the definitions and determination of the different potential terms. However, the essential features of the quantum confinement can be quantitatively accounted for if some simple analytical forms for these potentials are introduced, and in addition their relative strengths are properly accounted for.

The relative impact of the different potential terms depends on the extension of the confinement with respect to the characteristic lengths that are associated with these potential terms and determine their respective strengths. Whenever the confinement extension is larger than any of these lengths, the energy spectrum is determined by the corresponding potential term while the confinement only acts as a perturbation. If on the other hand, the confinement extension is less than these lengths, the roles are reversed and the confinement suppresses the different potential terms and imposes its own spectral distribution.[12, 13]

In the case of metals, it turns out that the confinement potential W completely dominates all other potentials. The reason for this is that the half filled band in metals, which is usually formed with s- and p- orbitals, can, for most purposes, be replaced by an equivalent pair of parabolic bands, situated on either side of the Fermi level, that are mirror images of each other and touch at $k = 0$. The wave vector dependent dielectric constant $\varepsilon(k)$ is infinite at $k = 0$, leading to the potentials V_{eh}, V_{mb}, and V_t being completely screened to within a distance $r_F = \frac{1}{k_F}$, which is of the order of a few angstroms, i.e. roughly equal to the lattice constant. Thus electrons and holes behave as free non-interacting particles over any distance in the perfect crystal.

The one-electron periodic Hamiltonian can therefore be replaced by the free electron and hole Hamiltonian, leading to the following equation

$$\left(-\frac{\hbar^2}{2m_e^*}\nabla_e^2 - \frac{\hbar^2}{2m_h^*}\nabla_h^2 + W\right)F(r_e,r_h) = EF(r_e,r_h)$$

(2.9)

17

The solution to this equation yields a significantly different eigenfunction and eigenenergy spectrum from the bulk. *i.e.*, the initially continuous energy spectrum of the free electron Hamiltonian is replaced by a discrete energy spectrum, namely one of quantum confined levels whose spacing depends on the extent of the confinement and can accordingly be modified as desired.

In spherical co-ordinates, equation 2.9 can be solved to give

$$F(r,\theta,\phi) = \left(\frac{2}{a^3}\right)^{1/2} \frac{1}{j_{l+1}(\alpha_{nl})} j_l\left(\alpha_{nl}\frac{r}{a}\right) Y_l^m(\theta,\phi) \tag{2.10}$$

$$= R_{nl} Y_l^m(\theta,\phi) \tag{2.11}$$

using the boundary condition $F(r = a) = 0$.

j_l is the spherical bessel function of order l, α_{nl} is its nth zero and $Y_l^m(\theta,\phi)$ are the spherical harmonics. The energy of the state given by quantum numbers n, l and m is,

$$E_{nl} = (\alpha_{nl})^2 E_0 \tag{2.12}$$

where $E_0 = \dfrac{\hbar^2}{2ma^2}$ is the ground state energy.

2.3.2 DIELECTRIC CONFINEMENT :

Despite their disparity, all composite materials that are formed by uniformly dispersed metal or semiconductor crystallites in a liquid or solid transparent dielectric share an important feature that has an essential impact on their properties in the optical frequency range: because the size of the crystallites is much smaller than the incident wavelength and their dielectric constant is very different from that of the surrounding transparent dielectric, the electric field that acts on and polarises the charges of these crystallites can be completely different from the macroscopic Maxwell field. This effect is known as the dielectric confinement effect.

2.3.2.1 LINEAR REGIME :

In general, the metallic crystallites embedded in the dielectric are not completely uniform either in size or in shape. However, in order to explain the essential features of dielectric confinement several features of the composite material can be considerably simplified. Firstly, it can be assumed that the surrounding host dielectric, liquid or solid, is an ideal isotropic dielectric of dielectric constant ε_h with the metal particles

uniformly and randomly distributed in small volume concentration in it. They are assumed to be spherical in shape, with a diameter d = 2a that is much smaller than the optical wavelength λ.
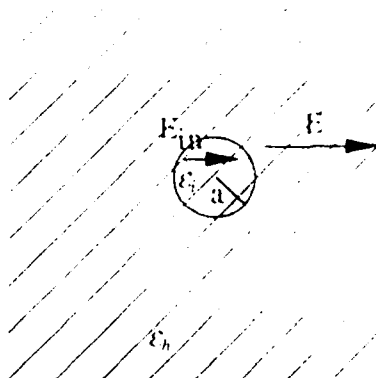

Figure 2.4 : A small sphere of dielectric constant ε_i embedded in a matrix of dielectric constant ε_h.

In the linear regime the relevant optical coefficient of such a crystallite or inclusion, of volume V, is the polarizability α_V and its dielectric constant ε_i can be defined by the relation,

$$\varepsilon_i = 1 + 4\pi\chi_i^{(1)} = 1 + 4\pi\frac{\alpha_V}{V} \tag{2.13}$$

where $\chi_i^{(1)}$ is the linear susceptibility.

The dielectric constant is expected to be a function of the particle size. Its limit for large particles is the bulk value ε_B.

Secondly, if it is assumed that the volume density of the particles in the dielectric, p, is so small that the interaction of the induced dipole moments on the particles can be ignored, then an effective dielectric constant ε for the composite medium can be introduced, whose relation to ε_h, ε_i, and p is given by the Maxwell-Garnet expression,[6]

$$\frac{\varepsilon - \varepsilon_h}{\varepsilon + 2\varepsilon_h} = p\frac{\varepsilon_i - \varepsilon_h}{\varepsilon_i + 2\varepsilon_h} \tag{2.14}$$

This relation is a straightforward consequence of the Clausius-Mossotti approximation for the local field corrections for spherical polarizable particles [26].For $p << 1$ it reduces to,

$$\varepsilon = \varepsilon_t + 3p\varepsilon_h \left(\frac{\varepsilon_t - \varepsilon_h}{\varepsilon_t + 2\varepsilon_h} \right) \tag{2.15}$$

Equation 2.14 can be derived from Lorentz-Lorenz local field arguments as follows:

Consider a collection of molecules subjected to an external electric field, $\vec{E}$. The dipole moment induced in any one of the molecules is given by,

$$\vec{\mu} = \alpha \vec{E}_{local} \tag{2.16}$$

where $\vec{E}_{local}$ is the Lorentz local field, which consists of the external field and the field due to the other molecules, and α is the linear polarizability.

$$\vec{E}_{local} = \vec{E} + \frac{4\pi}{3}\vec{P} \tag{2.17}$$

and $\vec{P}$ is the induced polarisation.

If the number of molecules $= N$, then,

$$\vec{P} = N\vec{\mu} = N\alpha\vec{E}_{local} = N\alpha\left(\vec{E} + \frac{4\pi}{3}\vec{P} \right) \tag{2.18}$$

or

$$\vec{P} = \frac{N\alpha}{1 - \frac{4\pi}{3}N\alpha}\vec{E} \equiv \chi^{(1)}\vec{E} \tag{2.19}$$

where,

$$\chi^{(1)} = \frac{N\alpha}{1 - \frac{4\pi}{3}N\alpha} \tag{2.20}$$

Equation 2.20 can be rewritten as,

$$\frac{\varepsilon^{(1)} - 1}{\varepsilon^{(1)} + 2} = \frac{4\pi}{3}N\alpha \tag{2.21}$$

where $\varepsilon^{(1)}$ is defined as,

$$\varepsilon^{(1)} = 1 + 4\pi\chi \qquad (2.22)$$

Equation 2.21 is the Lorentz-Lorenz law. It can alternatively be stated as,

$$\chi^{(1)} = \left(\frac{\varepsilon^{(1)} + 2}{3}\right) N\alpha \qquad (2.23)$$

or,

$$\vec{E}_{local} = \left(\frac{\varepsilon^{(1)} + 2}{3}\right)\vec{E} \qquad (2.24)$$

where $\left(\dfrac{\varepsilon^{(1)} + 2}{3}\right)$ is called the local field enhancement factor.

These arguments can also be applied to a composite material in the presence of a uniform electric field $\vec{E}$.[28, 29, 30] The polarisation induced in the material due to the external $\vec{E}$ field is given by,

$$\vec{P} = \chi_h \vec{E} + \vec{P}' \qquad (2.25)$$

where χ_h is the susceptibility of the host matrix and $\vec{P}'$ is the additional polarisation due to the inclusions.

$$\vec{P}' = N\vec{\mu} = N\varepsilon_h \alpha_i \vec{E}_l \qquad (2.26)$$

$\vec{\mu}$ is the dipole moment of the inclusions, $\alpha_i = a^3\left(\dfrac{\varepsilon_i - \varepsilon_h}{\varepsilon_i + 2\varepsilon_h}\right)$, is their polarizability and $\vec{E}_l$ is the local field, i.e., the field in their vicinity.

Just as in the derivation of the Lorentz-Lorenz law, one can write,

$$\vec{E}_l = \vec{E} + \frac{4\pi}{3\varepsilon_h}\vec{P}' \qquad (2.27)$$

which implies that,

$$\vec{P}' = \frac{N\varepsilon_h \alpha_i}{1 - \dfrac{4\pi}{3}N\alpha_i}\vec{E} \qquad (2.28)$$

Combining equations 2.25 and 2.28 one gets,

$$P = \chi_h E + \frac{N \varepsilon_i \alpha_i}{1 - \frac{4\pi}{3} N \alpha_i} E$$

(2.29)

$$P = \chi E \Rightarrow \chi = \chi_h + \frac{N \varepsilon_i \alpha_i}{1 - \frac{4\pi}{3} N \alpha_i}$$

(2.30)

Using the definition, $\varepsilon = 1 + 4\pi\chi$, for the dielectric constant, equation 2.30 can be alternatively expressed as :

$$\frac{\varepsilon - \varepsilon_h}{\varepsilon + 2\varepsilon_h} = p\left(\frac{\varepsilon_i - \varepsilon_h}{\varepsilon_i + 2\varepsilon_h} \right)$$

(2.31)

which is the same as equation 2.14.

ε_i is complex, $\varepsilon_i = \varepsilon_i' + i\varepsilon_i''$, and frequency dependent. It can be seen that the expression in equation 2.31 shows an enhancement close to the frequency ω_s, such that,

$$\varepsilon_i'(\omega_s) + 2\varepsilon_h = 0$$

(2.32)

which is the condition for the surface excitation or surface plasmon resonance frequency. The width of this resonance is determined by ε_i''. The absorption coefficient as a function of wavelength can easily be calculated from equation 2.31. It is given by,

$$\alpha = \frac{18\pi}{\lambda} p \varepsilon_h^{3/2} \frac{\varepsilon_i''}{\left(\varepsilon_i' + 2\varepsilon_h \right)^2 + 2\varepsilon_i''^2}$$

(2.33)

which is the same as the result that is obtained using the Mie theory to calculate the optical constants of composite materials.

Combining equations 2.27, 2.28 and 2.31 it is possible to derive an explicit relation between the local field experienced by the inclusions and the external macroscopic which is given by,

$$\vec{E}_i = \frac{\varepsilon + 2\varepsilon_h}{3\varepsilon_h} \vec{E}$$

(2.34)

Similarly, the field *inside* the inclusions is related to the external field through,

$$E_{in} = \frac{\varepsilon + 2\varepsilon_h}{\varepsilon_i + 2\varepsilon_h} E$$

(2.35)

Combining equations 2.34 and 2.35 the field inside the inclusions can be expressed in terms of the local field as,

$$E_i = \frac{\varepsilon_i + 2\varepsilon_h}{3\varepsilon_h} E_{in} \Rightarrow E_{in} = f_1 E_i$$

(2.36)

where f_1 is called the local field enhancement factor. Equation 2.36 constitutes the main result of this section.

2.3.2.2 NONLINEAR REGIME :

In the presence of an intense electric field the polarisation induced in the crystallites may be written as,

$$\Delta P = P^{(1)} + P^{(2)} + P^{(3)} + ...,$$

(2.37)

where $P^{(n)}$ with $n > 1$ is the nonlinear polarisation term of order n. In the case of an isotropic composite with random distribution of inclusions $P^{(2n)} = 0$,

$$P^{(1)} = \chi^{(1)} E, \text{ and}$$

$$P^{(3)} = \chi^{(3)} EEE,$$

where $\chi^{(1)}$ and $\chi^{(3)}$ are the linear and third order effective susceptibilities of the composite material.

The term $P^{(3)}$ is related to third order effects, the most important of which is the intensity-dependent refractive index or the optical Kerr effect. This effect is involved in a wide variety of important processes, including self-focusing of a laser beam,[31] self-phase and frequency modulation,[32] "soliton" pulse propagation,[33] and "optical phase conjugation".[34] It can be described as an optically induced change of the optical dielectric constant, i.e.

$$\delta\varepsilon = 12\pi\chi^{(3)}|E(\omega)|^2$$

(2.38)

This change of ε contains contributions from both the surrounding dielectric and the embedded crystallites, denoted by $\delta\varepsilon_h$ and $\delta\varepsilon_i$ respectively. Close to the surface plasmon resonance frequency the contribution from the surrounding dielectric is

negligible compared to that from the crystallite, even for $p \sim 1$. Thus a change, $\delta \varepsilon_i$ of the dielectric constant of the inclusions will result in a change in ε, the dielectric constant of the composite given by.

$$\delta \varepsilon = p \left(\frac{3\varepsilon_h}{\varepsilon_i + 2\varepsilon_h} \right)^{.} \delta \varepsilon_i = p f_1^{.} \delta \varepsilon_i$$

(2.39)

The above equation is obtained by differentiating equation 2.15.

If the third order susceptibility relevant to the internal field within inclusions is designated by $\chi_i^{(3)}$ then by analogy to equation 2.38,

$$\delta \varepsilon_i = 12 \pi \chi_i^{(3)} |E_{in}|^2$$

(2.40)

Substituting for $\delta \varepsilon_i$ in equation 2.39 gives

$$\delta \varepsilon = p f_1^2 \delta \varepsilon_i = 12 p \pi |f_1|^2 f_1^2 \chi_i^{(3)} |E|^2$$

(2.41)

and,

$$\chi^{(3)} = p |f_1|^2 f_1^2 \chi_i^{(3)}$$

(2.42)

Thus it can be seen that the nonlinearity can be enhanced by an amount equal to the fourth power of the local field factor, close to the surface plasmon resonance frequency. As one moves away from this resonance frequency, the local field factor approaches unity. At this stage dielectric confinement plays no role in the enhancement of the nonlinearity.

Another important point to be noted in equation 2.42 is that the macroscopic susceptibility $\chi^{(3)}$ can also be enhanced by the intrinsic quantum confinement mediated enhancement of the susceptibility of the inclusions, $\chi_i^{(3)}$.

2.4 NONLINEAR OPTICAL PROPERTIES

The third order susceptibility of the inclusions, $\chi_i^{(3)}$, can be calculated using the quantum mechanical expression in equation 1.2 which is repeated here for convenience.

$$\chi_{\mu\alpha\beta\gamma}^{(3)}\left(-\omega_\sigma,\omega_1,\omega_2,\omega_3\right) = \frac{Ne^4}{\varepsilon_0 3!\hbar^3}\sum_{abcd}\rho_0(a) \times$$

$$\left\{\frac{\pi_{rs}^\mu \pi_{st}^\alpha \pi_{tu}^\beta \pi_{ur}^\gamma}{\left(\Omega_{ba}-\omega_1-\omega_2-\omega_3\right)\left(\Omega_{ca}-\omega_2-\omega_3\right)\left(\Omega_{da}-\omega_3\right)}+47 \text{ similar terms}\right\} \quad (2.43)$$

In order to calculate the susceptibility, the matrix elements of the transition dipole moment, π, must be known. They can be calculated using the relation $[H,r]=-i\left(\dfrac{\hbar}{m}\right)p$ where p is the momentum operator and $\pi=\left(\dfrac{e}{m}\right)p$

The radial part of r between two states r (quantum numbers n, l) and s (quantum numbers n', l+1) is given by,

$$\int_0^a r^2 dr R_{nl} r R_{n'l+1} \quad (2.44)$$

Substituting for R_{nl} from equation 2.11, changing the integration variable from r to $\dfrac{r}{a}=x$ and integrating by parts gives,

$$\int_0^a r^2 dr R_{nl} r R_{n'l+1} = \frac{4\alpha_{nl}\alpha_{n'l+1}}{\left(\alpha_{nl}^2-\alpha_{n'l+1}^2\right)}a = 4aE_0 \frac{\left(E_{nl}E_{n'l+1}\right)^{1/2}}{\left(E_{n'l+1}-E_{nl}\right)^2} \quad (2.45)$$

Therefore the radial part of the π matrix element is

$$\pi_{rs} = \frac{4aeE_0}{i\hbar}\frac{\left(E_r E_s\right)^{1/2}}{E_s-E_r} \quad (2.46)$$

With these transition dipole moment elements it is possible to calculate the third order susceptibility, $\chi^{(3)}$, of the composite materials using the expression in equation 2.43. If the experiments are performed in the vicinity of a resonance, only a few of the elements are significant.

The susceptibility of the inclusions consists of three main contributions. The first contribution, called the intraband contribution, is caused by transitions within the s-p conduction band. It is mainly imaginary and negative and shows a strong size dependence. This is to be expected since the highly delocalised electrons in the conduction band would be greatly affected by a decrease in their delocalisation lengths due to quantum confinement. The second contribution, called the interband contribution, is due to transitions from the d - valence band to the s-p conduction band. It is also mainly imaginary and negative but is independent of the size of the inclusions. There are two main reasons for this. Firstly, the d - band electrons have a much greater effective mass than free electrons. Secondly they are already localised and are consequently unaffected by the quantum confinement. The last contribution, called the hot electron contribution, arises due to a change in the Fermi-Dirac distribution of electrons, about the Fermi level, caused by their increase in temperature on absorbing energy in a resonant process. This contribution is imaginary, like the first two, but it is positive. In the chapters following this one, several experiments are described which were undertaken in order evaluate the magnitude of the different contributions to $\chi_i^{(3)}$ and to ascertain which one, if any, was the dominant one.

The next three sections of this chapter are devoted to a detailed discussion of the three different contributions.

2.4.1 THE INTRABAND CONTRIBUTION :

Equation 2.43 for the calculation of $\chi^{(3)}$ in terms of the transition dipole moment matrix elements contains 48 terms. Keeping only those terms for which one of the factors in the denominator is equal to i / T_1, where T_1 is the lifetime of the states, the number of terms reduces to 32; 16 different terms, each appearing twice.

Considering the different components of the $\chi^{(3)}$ tensor, the terms can be divided into three groups : eight terms in $\chi_1^{(3)}$, four terms in $\chi_2^{(3)}$, and four terms in $\chi_3^{(3)}$, such that,

$$\chi_{uuu}^{(3)} = 2\left(\chi_1^{(3)} + \chi_2^{(3)} + \chi_3^{(3)}\right) \tag{2.47a}$$

$$\chi_{uvv}^{(3)} = 2\left(\varepsilon_{uvv}\chi_1^{(3)} + \varepsilon_{uvv}\chi_2^{(3)} + \varepsilon_{uvv}\chi_3^{(3)}\right) \tag{2.47b}$$

$$\chi_{uvu}^{(3)} = \chi_{uuv}^{(3)} = \varepsilon_{uvv}\left(\chi_2^{(3)} + \chi_3^{(3)}\right) + \varepsilon_{uvv}\left(\chi_1^{(3)} + \chi_3^{(3)}\right) + \varepsilon_{uvv}\left(\chi_1^{(3)} + \chi_2^{(3)}\right) \tag{2.47c}$$

where ε_{ijkl} is a corrective multiplicative factor when $(ijkl) \neq (xxxx)$ and

$$F_{\text{uuu}} + F_{\text{uuu}} + F_{\text{uuu}} = 1 \qquad (2.48)$$

For a two level system consisting of initial and final states, r and s, $\chi_1^{(3)}$ is given by,

$$\chi_1^{(3)} = -\frac{2}{3} V \frac{T_1}{T_2} A \sum_{r,s} \frac{|\pi_{r,s}|^4}{\omega^4} \left\{ \frac{1}{\left(\omega_{sr} - \omega - iT_2^{-1} \right)\left[\left(\omega_{sr} - \omega \right)^2 + T_2^{-2} \right]} + \right.$$

$$\left. \frac{1}{\left(\omega_{sr} + \omega + iT_2^{-1} \right)\left[\left(\omega_{sr} + \omega \right)^2 + T_2^{-2} \right]} \right\} \qquad (2.49)$$

where V is the volume of the crystallite, T_2 is the dephasing time, A is an angular form factor, $\pi_{r,s}$ is defined by equation 2.46 and $\omega_{sr} = \left(E_s - E_r \right)$, setting $h = 1$ for convenience.

There are two main contributions to $\chi_1^{(3)}$. The first one arises when $\omega \approx E_s - E_r$, and the second one when $E_s \approx E_r$. In the first case it is only necessary to consider the first term in equation 2.49 since its contribution dominates that of the second term. In the second case, both terms need to be considered. However, it turns out that the overall contribution to $\chi_1^{(3)}$ in this case is much less than the in first case and it can be safely ignored.

Substituting for $\pi_{r,s}$ from equation 2.46, equation 2.49 can be rewritten as,

$$\chi_1^{(3)} = -\frac{2}{3} V \frac{T_1}{T_2} \frac{1}{\omega^4} A \left(4aeE_0 \right)^4 \sum_{r,s} \frac{\left(E_r E_s \right)^2}{\left(E_r - E_s \right)^4} \ \times$$

$$\left\{ \frac{1}{\left(E_s - E_r - \omega - iT_2^{-1} \right)\left[\left(E_s - E_r - \omega \right)^2 + T_2^{-2} \right]} \right\} \qquad (2.50)$$

for the case when $\omega_{sr} = \left(E_s - E_r \right)$. The summation in the above equation can be replaced by an integral to give,

27

$$\chi_1 = -\frac{2}{3} V \frac{T_1}{T_2} \frac{1}{\omega^4} A (4ae E_0)^4 \int_0^t \upsilon(E) dE \int \frac{1}{2\Delta E} dE$$

$$\left| \frac{E \cdot E}{(E - E)^2} \frac{1}{(E - E - \omega - iT_2^{-1})\left[(E - E - \omega)^2 + T_2^{-2}\right]} \right| \qquad (2.51)$$

where $\upsilon(E)$ is the density of states. In the second integral, the density $\frac{1}{2\Delta E}$ takes into account the fact that the l number of the s state is determined by the l number of the r state and is of different parity.

Equation 2.51 can be solved to give,

$$\chi_1^{(3)} = -i \frac{V}{9\pi} A T_1 T_2 \frac{(4ae)^4}{\omega^7} E_0^2 E_f^4 g_1(v) \qquad (2.52)$$

with $v = \frac{\omega}{E_f}$ and $g_1(v) = \frac{1}{v} \int_{1-v}^1 x^{5/2}(x+v)^{3/2} dx$.

The quantum mechanical expressions for $\chi_2^{(3)}$ and $\chi_3^{(3)}$ are given by,

$$\chi_2^{(3)} = \frac{1}{3} V \frac{T_1}{T_2} A \sum_{r,s,t} \frac{|\pi_{rs}|^2 |\pi_{st}|^2}{\omega^4} \left\{ \frac{1}{(\omega_{ts} - \omega - iT_2^{-1})\left[(\omega_{sr} - \omega)^2 + T_2^{-2}\right]} \right.$$

$$\left. + \frac{1}{(\omega_{ts} + \omega + iT_2^{-1})\left[(\omega_{sr} + \omega)^2 + T_2^{-2}\right]} \right\} \qquad (2.53)$$

and

$$\chi_3^{(3)} = -\frac{1}{3} V \frac{T_1}{T_2} A \sum_{r,s,u} \frac{|\pi_{rs}|^2 |\pi_{ru}|^2}{\omega^4} \left\{ \frac{1}{(\omega_{ur} - \omega - iT_2^{-1})\left[(\omega_{sr} + \omega)^2 + T_2^{-2}\right]} \right.$$

$$\left. + \frac{1}{(\omega_{ur} + \omega + iT_2^{-1})\left[(\omega_{sr} - \omega)^2 + T_2^{-2}\right]} \right\} \qquad (2.54)$$

28

The only important contribution to $\chi_2^{(3)}$ is when ω_{ts} and ω_{sr} are close to ω. In this case it is only necessary to consider the first term of equation 2.53, and by proceeding in the same way as for $\chi_1^{(3)}$, the final result obtained is,

$$\chi_2^{(3)} = i \frac{V}{18\pi} A' T_1 \frac{(4ae)^4}{\omega^7} E_0^{3/2} E_f^{7/2} g_2(v) \tag{2.55}$$

with

$$g_2(v) = \frac{1}{v} \int_{1-v}^{1} x^{1/2} (x+v)^{1/2} (x+2v)^{1/2} dx \tag{2.56}$$

Similarly, for $\chi_3^{(3)}$, the only important contribution is when ω_{sr} and ω_{ru} are close to ω, which means that the first term in equation 2.54 can be ignored, giving,

$$\chi_3^{(3)} = i \frac{V}{18\pi} A' T_1 \frac{(4ae)^4}{\omega^7} E_0^{3/2} E_f^{7/2} g_3(v) \tag{2.57}$$

with

$$g_3(v) = \frac{1}{v} \int_{x_0}^{1} x^{5/2} (x+v)^{1/2} (x-v)^{1/2} dx \tag{2.58}$$

where $x_0 = \max(v, 1-v)$.

Combining equations 2.47a, 2.52, 2.55 and 2.57 yields,

$$\chi_{xxx}^{(3)} = 2\chi_1^{(3)} \left[1 - \frac{a}{T_2} \left(\frac{m}{2E_f} \right)^{1/2} \frac{g_2(v) + g_3(v)}{g_1(v)} \right] \tag{2.59}$$

$$= 2\chi_1^{(3)} \left[1 - \frac{a}{a_0} \right] \tag{2.60}$$

where,

$$a_0 = T_2 \left(\frac{2E_f}{m} \right)^{1/2} \frac{g_1(v)}{g_2(v) + g_3(v)} \tag{2.61}$$

or, substituting for $\chi_1^{(3)}$,

$$\chi_{xxx}^{(3)} = 0.144iT_1T_2 \frac{1}{a^2} \frac{e^4}{m^2\hbar^3\omega^7} E_f^2 g_1(v)\left(1 - \frac{a}{a_0}\right) \tag{2.62}$$

$$= -\frac{0.144i}{\tau_0} T_1 T_2 \frac{1}{a^2} \frac{e^4}{m^2\hbar^3\omega^7} E_f^2 g_1(v)\left(1 - \frac{a}{a_0}\right) \tag{2.63}$$

in SI units.

When $a = a_0$, $\chi_{xxx}^{(3)} \to 0$.

When $a \ll a_0$, $\chi_{xxx}^{(3)} \propto a^2$.

When $a \gg a_0$, $\chi_{xxx}^{(3)} \propto a^3$

For the case of gold, with $E_f = 5.5ev$ and setting $T_2 = 20fs$, $a_0 \approx 136\text{Å}$.

The magnitude of $\chi^{(3)}$ can be approximated by inserting suitable values for the physical parameters in equation 2.63 above. Setting $T_1 = 0.5ps$ and $\omega = 3.55 \times 10^{15}s^{-1}$ yields, $\left|\chi^{(3)}\right| \approx 4.23 \times 10^{-18} m^2 V^{-2}$.

2.4.2 THE INTERBAND CONTRIBUTION :

2.4.2.1 LINEAR REGIME :

It is well known that the generation of an optical plasma, due to interband transitions, can result in a strong modification of the dielectric function $\varepsilon(\omega)$ in a semiconductor.[36] The same argument can be applied to the metallic crystallites in the composite material. According to the Drude theory of metals,[37, 38] the complex dielectric constant of a free electron metal, to a first approximation, is given by

$$\varepsilon(\omega) = 1 - \frac{\omega_p^2}{\omega^2} \tag{2.64}$$

where $\omega_p^2 = \frac{4\pi ne^2}{m}$ is the plasma frequency, with n, e and m being the electronic concentration, charge and mass respectively.

In the case of alkali metals, there is a striking correspondence between theory and experiment, in this respect. In other metals, however, different contributions to the dielectric constant compete quite substantially with the Drude term.

The dielectric constant of noble metals consists of two terms: one due to intraband transitions within the s - p conduction band and the other due to interband transitions from the d - valence band to the s - p conduction band.

$$\varepsilon_i(\omega) = \varepsilon_{intra} + \varepsilon_{inter} \tag{2.65}$$

The free electron intraband term corresponds to the Drude dielectric constant, i.e.,

$$\varepsilon_{intra} = \frac{-\omega_p^2}{\omega\left(\omega + i / \tau_{eff}\right)} \tag{2.66}$$

where τ_{eff} is the mean collision time for free electrons taking the surface into account. In the large sphere limit τ_{eff} reduces to $T_2 / 2$.

The imaginary part of ε_{inter} is dependent on the joint density of states involved in the transition and on the momentum operator between the states. It is given by,

$$\varepsilon_{inter}^{"} = \frac{4\pi^2 e^2}{3m^2\omega^2} \sum_{i,j} \int \frac{dk}{4\pi^3} \left|P_{ij}(k)\right|^2 f_i(k)\left(1 - f_j(k)\right)\delta\left(E_j(k) - E_i(k) - \hbar\omega\right) \tag{2.67}$$

$P_{ij}(k)$ is the matrix element of the momentum operator between states corresponding the quasi momentum $\hbar k$, f_i and f_j are the occupation numbers and E_i and E_j are the energies of the initial and final levels. Near the surface plasma resonance frequency, the sum over the indices i and j is dominated by one term whose initial state is the top of the valence band and final state is the conduction band. Since the integral in k space is dominated by the vicinity of the X point of the Brillouin zone where the band gap is 1.7eV, (See figure 2.5) the dependence of $P_{ij}(k)$ is weak and it can be approximated to be a constant P. Equation 2.67 can then be rewritten as,

$$\varepsilon_{inter}^{"} = \frac{4\pi^2 e^2}{3m^2\omega^2} |P|^2 J(\omega) \tag{2.68}$$

and the corresponding absorption coefficient $\alpha(\omega)$ is given by,

$$\alpha(\omega) = \frac{\omega}{n(\omega)c} \varepsilon_{inter}^{"} \tag{2.69}$$

$J(\omega)$ is the joint density of states. In thermal equilibrium the contribution to the electronic density from electrons in the nth band with wave vectors in the infinitesimal volume element dk of k space is given by the Fermi distribution

Band structure of gold (fig. 2.5) Reference 2.39

$$f(T) = \frac{1}{1 + e^{-\frac{\delta E}{k_B T}}} \tag{2.70}$$

with $\delta E = E_F - (E_d + \hbar\omega)$, where E_d is the d-band energy. k_B is Boltzmanns constant and T is the temperature.

The joint density of states is therefore given by,

$$J(\omega) = \sum_{i,j} \int \frac{dk}{4\pi^3} f_i(k)(1 - f_j(k)) \delta(E_j(k) - E_i(k) - \hbar\omega) \tag{2.71}$$

NONLINEAR REGIME :

If the excitation frequency used is resonant with a particular interband transition, the main contribution to $\chi^{(3)}$ will consist of the contribution of the two levels involved in that transition. Since it is resonant, it will be mostly imaginary with the imaginary part given by [8, 35] ???

$$\mathrm{Im}\,\chi^{(3)}_{inter} = -\frac{4}{3} A \frac{T_1}{T_2} \frac{e^4}{m^4 \omega^4} \sum_{i,j} \int \frac{d^3 k}{4\pi^3} |P_{ij}(k)|^4$$

$$\times f_i(k)(1 - f_j(k)) \frac{\pi T_2^2}{2\hbar^2} \delta(E_j(k) - E_i(k) - \hbar\omega) \tag{2.72}$$

Where T_1 and T_2 are the energy lifetime and dephasing time corresponding to the two level system and A is an angular form factor $\approx 1/5$.

Since only contributions from the X point of the Brillouin zone are relevant to the integral in equation 2.72, by analogy to equation 2.68, equation 2.72 can be rewritten as,

$$\mathrm{Im}\,\chi^{(3)}_{inter} = -\frac{2\pi}{3} A T_1 T_2 \frac{e^4}{\hbar^2 m^4 \omega^4} |P|^4 J(\omega) \tag{2.73}$$

The product $J(\omega)|P|^2$ can be obtained from the value of ε_{inter} which in turn can be obtained by subtracting the Drude term from the overall dielectric constant. $|P|^2$ is given by the expression [40]

$$|P|^2 = \left(\frac{G\hbar\omega_g}{2\omega}\right)^2 \tag{2.74}$$

33

where G is the modulus of the reciprocal lattice wave vector relevant to the transition and $\hbar\omega_g$ is the gap energy. Taking $\varepsilon_{inter} = 1.9$, $G = 1.5\times10^8\,cm^{-1}$ (from the point X in the Brillouin zone) and $\omega = 3.55\times10^{15}\,s^{-1}$ (surface plasmon resonance frequency), gives

$$|P|^2 = \times10^{-49}\left(kg\ m\ s^{-1}\right)^2 \qquad (2.75)$$

and

$$\operatorname{Im}\chi^{(3)}_{inter} = -1.8\times10^{-17}\,m^2\,V^{-2} \qquad (2.76)$$

In order to obtain the result in equation 2.76, the values for T_1 and T_2 were approximated to be 2×10^{-11} and 2×10^{-14} respectively.[8]

This contribution to $\chi^{(3)}$ is size independent down to very small sizes. The reason for this is that the quantum size effect should be unobservable for the d - levels because of their large effective masses and the fact that the electrons already have a localised character. The calculation of the interband contribution is affected by s-p band only for very small spheres with sizes less than 2.5nm.[41, 42]

Thus, in this case, the contribution to $\chi^{(3)}$ is approximately an order of magnitude greater than that due to intraband transitions.

2.4.3 THE HOT ELECTRON CONTRIBUTION :

The third mechanism contributing to the susceptibility of the inclusions is the hot electron contribution. It results from the modification of the population of the electron states, the Fermi-Dirac distribution, caused by the elevation of their temperatures subsequent to the absorption of photons in the resonant process, but before the heat is released to the lattice of the crystallite; this leads to a contribution to $\chi^{(3)}$ that is positive, imaginary and size independent.[9, 10, 12, 13]

Because the specific heat of the conduction electrons is weak, on the absorption of photons they can heat up to a temperature that is much higher than that of the lattice. It has been shown that it takes a few ps for these hot electrons to come back into thermal equilibrium with the lattice.[43, 44] During this time, their Fermi-Dirac distribution gets modified resulting in part of the one-electron levels below the Fermi level being emptied and part of the one-electron levels above the Fermi level being occupied. This leads to a modification of the dielectric constant of the inclusions and consequently contributes to the overall susceptibility.

The energy of the photons in the vicinity of the surface plasmon resonance frequency is very close to the band gap which exists in gold near the L point of the Brillouin zone ($\hbar\omega_g = 2.4eV$) and therefore this effect is very strong. The relevant part of the total dielectric function is called ε_l and its imaginary part is given by,[10]

$$\varepsilon_l^{\cdot} = C(1 - f(T))$$ (2.77)

where $f(T)$ is the occupation number of the conduction electrons and C is a temperature independent constant.

The change in the dielectric function as a function of temperature is obtained by differentiating equation 2.77 :

$$\frac{\partial \varepsilon_L^{\cdot}}{\partial T} = C \frac{\delta E}{k_B T^2} \exp\left(\frac{-\delta E}{k_B T}\right) f(T)^2$$ (2.78)

Setting $\hbar\omega_g$ to 2.43 eV and $C \approx 12$ leads to the following estimate,

$$\frac{\partial \varepsilon_L^{\cdot}}{\partial T} = 2.9 \times 10^{-3} K^{-1}$$ (2.79)

At room temperature $f(T) \to 1$ which implies that $\varepsilon_L^{\cdot} \to 0$. If the temperature of the conduction electrons *changes*, then the change in $\varepsilon_l^{\cdot}$ results in a change in the overall dielectric constant of the inclusions, ε_i, given by,

$$\delta\varepsilon_i = \frac{\partial \varepsilon_L^{\cdot}}{\partial T} \delta T$$ (2.80)

where δT is the change in temperature of the conduction electrons. It is related to the energy absorbed E_{abs}, and the specific heat γT, of the electrons and can be calculated using,

$$\delta T = \frac{E_{abs}}{\gamma T}$$ (2.81)

The energy absorbed per unit volume of metal by the free electrons is,

$$E_{abs} = |f_1|^2 \varepsilon_D^{\cdot} \tau_0 I_0 \frac{\omega}{nc}$$ (2.82)

where f is the local field factor, ε_D is the imaginary part of the Drude contribution to the dielectric constant, τ_0 is the time constant for the cooling of the electrons, I_0 is the incident laser energy and n is the refractive index of the composite material.

The quantity $\varepsilon_D \tau_0$ in equation 2.82 is given by,

$$\varepsilon_D \tau_0 = \frac{\omega_p}{\omega^2} \frac{\tau_0}{\tau_{eff}} \tag{2.83}$$

where ω_p is the plasma frequency and the ratio $\dfrac{\tau_0}{\tau_{eff}}$ is equal to the number of collisions an electron has to undergo in order to transfer its excess energy, either to the metallic particle phonons or the phonons of the surrounding dielectric through the interface. If the excess energy is 2.33 eV ($\hbar\omega$) and each collision, on average, transfers 0.02eV, then the total number of collisions required is approximately 120.[43] Taking $\omega_p = 3.49 \times 10^{15} s^{-1}$ gives $\varepsilon_D \tau_0 = 3.3 \times 10^{-4} s$.

Combining equations 2.79, 2.80, 2.81 and 2.82 gives an expression for the change in the dielectric constant of the inclusions which is related to their susceptibility:

$$\delta\varepsilon_i = \frac{\partial \varepsilon_L}{\partial T} |f_i|^2 \varepsilon_D \tau_0 I_0 \frac{\omega}{nc\gamma\Gamma} \frac{24\pi^2}{24\pi^2} \tag{2.84}$$

$$= \frac{24\pi^2}{nc} \chi^{(3)} |f_i|^2 I_0 \tag{2.85}$$

where

$$\chi^{(3)} = \frac{\partial \varepsilon_L}{\partial T} \frac{\varepsilon_D \tau_0}{\gamma\Gamma} \frac{1}{24\pi^2} \tag{2.86}$$

Using $\gamma = 66 Jm^{-3}K^{-2}$,[26] gives

$$\chi^{(3)} = 10^{-8} esu = 1.5 \times 10^{-16} m^2 V^{-2} \tag{2.87}$$

depending on the wavelength of the exciting radiation.

The contribution is mainly imaginary. Contrary to the first two, its sign is positive. Also, it is an order of magnitude greater than the interband contribution which is, in turn, an order of magnitude greater than the intraband contribution.

CONCLUSIONS

From this chapter the obvious conclusion would be that in an experimental situation, the hot electron contribution would be the dominant one followed by the interband and intraband contributions, in that order.

This, however, is not strictly true. The numbers obtained are only approximate as a lot of the parameters in the equations are not known to a sufficient degree of accuracy and do not merit such a statement. It should be possible, though, to determine experimentally, from the sign and the response time of the susceptibility, the physical mechanism responsible for the process.

The following four chapters describe different experimental techniques for determining $\chi^{(3)}$ and, hopefully, the physics underlying it.

REFERENCES

2.1   Chemla. D.S. and Zyss, J. eds. (1987) *Nonlinear Optical Properties of Organic Molecules and Crystals. Quadratic Nonlinear Optic Effects.* Orlando : Academic Press.

2.2   Gibbs. H.M. (1985) *Optical Bistability : Controlling Light with Light.* Orlando: Academic Press.

2.3   Halperin, W.P. (1986) *Quantum Size Effects in Metal Particles* Rev. Mod. Phys **58**, 533.

2.4   Perenboom, J.A.A.J., Wyder, P. and Meier, F. (1981) *Electronic Properties of Small Metallic Particles.* Phys. Rep. **78**, 173.

2.5   Mie, G. (1908) Ann. Phys. **25**, 337

2.6   Maxwell Garnett

2.7   Ricard, D., Roussignol, Ph. and Flytzanis, C. (1985) *Surface mediated enhancement of Optical phase conjugation in Metal Colloids.* Optics Letters, **10**, No. 10, 511 - 513.

2.8   Hache, F., Ricard, D. and Flytzanis, C. (1986) *Optical Nonlinearities of Small Metal Particles : Surface-mediated Resonance and Quantum Size Effects.* J. Opt. Soc. Am. B, **3**, No. 12, 1647 - 1455.

2.9   Hache, F., Ricard, D., Flytzanis, C and Kreibig, U. (1988) *The Optical Kerr Effect in Small Metal Particles and Metal Colloids : The Case of Gold.* Appl. Phys. A. **47**, 347 - 357.

2.10   Hache, F., Ricard, D. and Flytzanis, C (1989) *The Optical Kerr Effect in Small Metal Particles and Metal -doped glasses : The Case of Gold.* SPIE Vol. 1127 Nonlinear Optical Materials II, 115 - 122.

2.11   Bloemer, M.J., Haus, H.W. and Ashley, P.R. (1990) *Degenerate Four Wave Mixing in Colloidal Gold as a Function of Particle Size.* J. Opt. Soc. Am. B, **7**, No.5, 790 - 795.

2.12   Flytzanis, C., Hache, F., Klein, M.C., Ricard, D. and Roussignol, Ph. (1991) *Nonlinear Optics in Composite Materials.* Progress in Optics **29**, 321 - 411.

2.13   Flytzanis, C. and Hutter, H. (1992) *Nonlinear Optics in Quantum Confined Structures*. Contemporary Nonlinear Optics : Academic Press, 297 - 365.

2.14   Flytzanis, C., Hache, F., Ricard, D. and Roussignol, Ph. (1986) *Physics and Fabrication of Microstructures and Microdevices*. Berlin : Springer-Verlag, eds. M.J. Kelly and C. Weisbuch, 331 - 342.

2.15   Frens, G. (1973) *Controlled nucleation for the regulation of particle size in monodisperse gold suspensions*, Nature Phys. Sci. **241**, 20 - 22.

2.16   Duff, D. (1989) PhD. thesis, Pembroke College, University of Cambridge.

2.17   Turkavich, J., Stevenson, P. C. and Hillier, J. (1951) Disc. Farad. Soc. **11**, 55 - 75.

2.18   Doyle, W.T. (1960) Proc. Phys. Soc. 75, 649.

2.19   Johnson, P. B. and Christy, R. W. (1972) *Optical Constants of the Noble Metals*, Phys. Rev. B **6**, 4370 - 4379.

2.20   Bloemer, M. J., Buncick, M. C., Warmack, R. J. and Ferrell, T. L. (1988) *Surface electromagnetic modes in prolate spheroids of gold, aluminium and copper*, J. Opt. Soc. Am. B **5**, 2552.

2.21   Kreibig, U. (1978) *Lattice defects in small metal particles and their influence on size effects*, Z. phys. B **31**, 39.

2.22   Berry, C. R. and Skillman, D. C. (1969) J. Photogr. Sci. **17**, 145.

2.23   Marzke, R. F. (1979) Catal. Rev. Sci. Eng. **19**, 43.

2.24   Papavassiliou, G. C. (1980) *Optical properties of small inorganic and organic metal particles*, Prog. Solid State Chem. **12**, 185.

2.25   Frölich,

2.26   Ashcroft, N. W. and Mermin, N. D. (1976) *Solid State Physics*, Holt, New York.

2.27   Cross, J.A. (1987) *ELECTROSTATICS : Principles, Problems and Applications*, Adam Hilger, 425-491.

2.28 Sipe, J. E. and Boyd, R. W. (1992) *Nonlinear susceptibility of composite optical materials in the Maxwell Garnett model*, Phys. Rev. A **46**, 1614 - 1629.

2.29 Boyd, R. W. (1992) *Enhancement of Nonlinear Optical Susceptibilities through Local Field Effects*, Presented at Allied Signal Inc., Research and Technology.

2.30 maki, J. J., Malcuit, M. S., Sipe, J. E. and Boyd, R. W. (1991) *Linear and Nonlinear Optical measurements of the Lorentz Local Field*, Phys. Rev. Lett. **67**, 972 - 975.

2.31 Sheik-bahae, M., Said, A. A. and van Stryland, E. W. (1989) *High Sensitivity, Single Beam n₂ Measurements*, Opt. Lett. **14**, 955

2.32

2.33

2.34 Yariv, A. (1978) *Phase Conjugate Optics and Real-Time Holography*, IEEE J. Quant. Elec. **QE 14**, 650 - 660

2.35 Hache, F. (1988) *Effet Kerr optique dans les petites sphéres et les colloïdes métalliques : étude théorique et expérimentale dans le cas de l'or*, PhD. thesis, Universite De Paris-Sud.

2.36 Jain, R. K. and Klein, M. B. (1983) *Degenerate Four-Wave Mixing in Semiconductors*, in *Optical Phase Conjugation*, ed. Fisher, R. A., Academic Press, Inc..

2.37 Drude (1900) Annalen der physik **1**, 566

2.38 Drude (1900) Annalen der physik **3**,369

2.39 Christensen, N. E. and Seraphin, B. O. (1971) *Relativistic band Calculation and the Optical Properties of Gold*, Phys. rev. B **4**, 3321 - 3344.

2.40 Koyama, R. Y. and Smith, N. V. (1971) Phys Rev. B **2**, 3321

2.41 Kreibig, U. (1978) Solid State Commun. **28**, 767

2.42 Kreibig, U. (1980) in *Growth and Properties of metal Clusters*, ed. J. Bourdon, Elsevier, Amsterdam.

2.43   Eesley, G. L. (1986) *Generation of nonequilibrium lattice temperatures in copper by picosecond laser pulses*, Phys. rev. B **33**, 2144 - 2151.

2.44   Schoenlein, R. W., Lin, W. Z., Fujimoto, J. A. and Eesley, G. L. (1987) *Femtosecond studies of nonequilibrium electronic processes in metals*, Phys. Rev. Lett. **58**, 1680 -1683.

CHAPTER 3

INTENSITY DEPENDENT ABSORPTION MEASUREMENTS

Various experimental techniques are known for determining the real and imaginary parts of the third order susceptibility $\chi^{(3)}$, discussed in chapter 1. This chapter focuses on a method for evaluating these quantities in a nonlinear material by measuring, as a function of the incident light, the material's absorption and the phase change induced by it.[1, 2, 3] A completely linear material will show no change in absorption with intensity; materials that are "two photon (or multiphoton) absorbers" show an increase in absorption with increasing intensity and materials that are "saturable absorbers" show a decrease in absorption with increasing intensity.

EXPERIMENTAL TECHNIQUE

The experimental set-up is shown in figure 3.1. Using a Gaussian laser beam in tight-focus geometry, the transmittance of the nonlinear medium is measured, in the far field, as a function of its position Z, measured with respect to the focal plane of the lens. Such a trace is expected to be symmetric with respect to the focus, where there is either a minimum transmittance (e.g. multiphoton absorption) or a maximum transmittance (e.g. saturation of absorption). The coefficients of nonlinear absorption and hence the imaginary part of $\chi^{(3)}$ can be easily calculated from such a curve.

If an aperture is placed in front of the photodiode, it is possible to detect contributions from the real part of the susceptibility as well. This contribution causes the beam to be focused or defocused (depending on the sign of the nonlinearity) as it passes through the sample. Focusing of the beam, when the sample is on the positive side of the focal plane, causes increased aperture transmittance, while defocusing has the converse effect. If the sample is on the negative side of the focal plane, the situation is reversed. By subtracting the effect of the imaginary component from this curve (by using the first trace) it is possible to separately evaluate both the components of the nonlinear susceptibility.[4, 5]

The laser system used was a tuneable PRA Nitrogen pumped dye laser with 500ps pulses operating at a repetition rate of 5 Hz. The experiments were performed at two different wavelengths of 516nm and 522nm, which lie very close to the surface plasmon resonance frequency. The dye used was Coumarin 485. The output energy

from the laser at these wavelengths was ≈ $40\mu J$ and the beam was focused down to a spot size of ≈ $40\mu m$ giving a peak intensity of the order of $10^8 W / cm^2$.
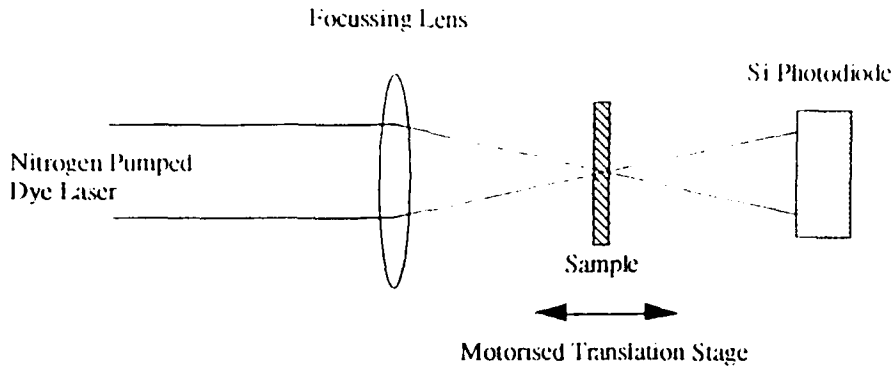

Figure 3.1 : Experimental Set-up for Intensity Dependent Absorption Measurements

GENERAL THEORY

The description of resonant optical processes is greatly simplified by restricting attention to the dominant resonant transition. The most widely used description is based on a model of a two level atom. If there is a distribution of transition frequencies between the levels the system is considered to be inhomogenously broadened. Saturated absorption spectroscopy is a useful tool for determining whether a material can be described by homogenous or inhomogenous saturation because the dependence of the absorption coefficient on intensity is different in both cases.[6] If the material can be described as a homogeneously broadened two level system then the variation of the absorption coefficient with intensity is given by :

$$\alpha(\omega) = \frac{\alpha_0(\omega)}{1 + \dfrac{I}{I_{sat}}}$$

(3.1)

where $\alpha_0(\omega)$, I and I_{sat} are the unsaturated absorption coefficient, the input intensity and the saturation intensity respectively.

For extremely inhomogenously broadened systems the expression for the absorption coefficient is modified to read :

$$\alpha(\omega) = \frac{\alpha_0(\omega)}{\left(1 + \dfrac{I}{I_{sat}}\right)^{1/2}}$$

(3.2)

In physical terms, the inhomogenous gain or absorption saturates more slowly at large intensities because the signal can draw energy from an increasingly wider range of packets as the signal intensity increases.

Equations 3.1 and 3.2 hold, provided that the contribution from the real part of the susceptibility can be ignored, i.e., there should be no aperture present in front of the signal photodiode.

The experiments, with no aperture, were performed on 10 different samples and the resultant data was fitted by a nonlinear least squares fit using both equations 3.1 and 3.2, with I_{sat} being the only fit parameter. In all the cases, equation 3.2 (i.e. the equation for inhomogenously broadened systems) gave a far superior fit. A typical result is shown in figure 3.2. The sample in the figure is an 18nm colloid dispersed in deionised water.
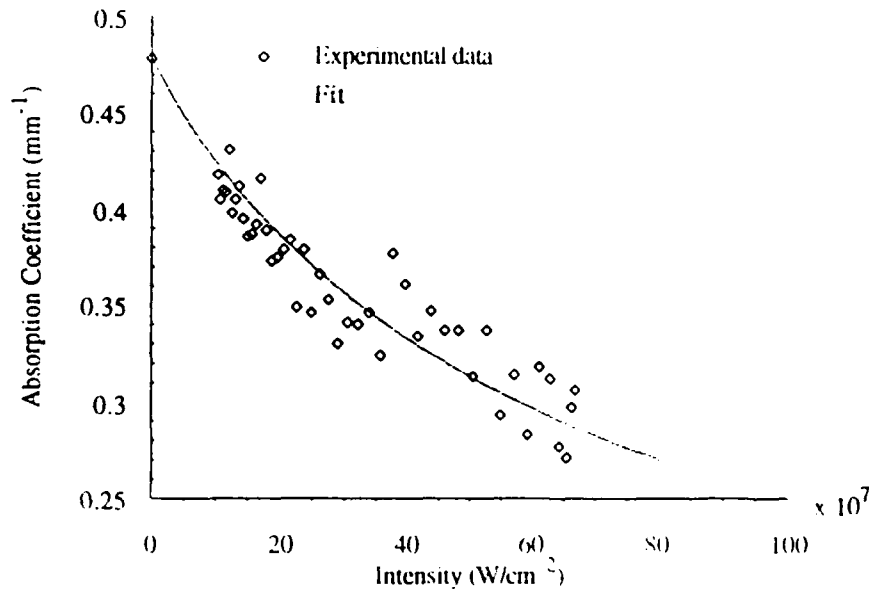

Figure 3.2 : Absorption Coefficient Vs Laser intensity. $\lambda = 522nm$

From the least squares fit it is possible to determine I_{sat} which is then used in the equation

$$\operatorname{Im}\chi^{(3)} = \frac{\varepsilon_0 c n_0^2 \alpha_0 \lambda}{2\pi I_{sat}}$$

(3.3)

to calculate the imaginary part of the third order susceptibility.

ε_0, n_0 and α_0 are the permittivity of free space, the linear index of refraction and the low intensity absorption coefficient of the sample respectively.

44

Equation 3.3 can be derived by starting from Maxwell's equations as follows :

For nonmagnetic, centrosymmetric materials, the polarisation induced by the incidence of an intense light source is given by

$$P = \varepsilon_0 \left(\chi^{'''} + \chi^{(3)} E.E \right) E$$

(3.4)

Using this expression in the equation for the displacement vector

$$D = \varepsilon_0 E + P$$

(3.5)

we get

$$D = \varepsilon_0 \left(1 + \chi^{(1)} + \chi^{(3)} E.E \right) E = \varepsilon_0 \left(\varepsilon_l + \varepsilon_{nl} \right) E$$

(3.6)

where $\varepsilon_l = 1 + \chi^{(1)}$ and $\varepsilon_{nl} = \chi^{(3)} E.E$, are the linear and nonlinear parts of the permittivity of the medium.

The refractive index of the material, n, will also undergo a change due to the incident light. This is expressed by

$$n = n_0 + n_2 I$$

(3.7)

where n_0 and n_2 are the linear and nonlinear indices of refraction.

Refractive index is related to the permittivity of the medium, ε, through

$$\varepsilon = n^2 = n_0^2 + 2n_0 n_2 I + \text{higher order terms}$$

(3.8)

Here $n_0^2 = \varepsilon_l$ and $2n_0 n_2 I = \varepsilon_{nl}$.

Thus,

$$2n_0 n_2 I = \chi^{(3)} E.E$$

(3.9)

which implies that,

$$n_2 = \frac{\chi^{(3)}}{2\varepsilon_0 c n_0^2}$$

(3.10)

since

$$I - \varepsilon_0 c n_0 E.E$$

For an absorbing material we have the equations

$$I = I_0 \exp(-\alpha z) \quad \text{and} \quad E = E_0 \exp(inkz)$$

(3.12)

where I_0 and E_0 are the incident light intensity and electric field respectively. α is the linear absorption coefficient and k is the wave vector.

From equation 3.12 we get

$$\alpha = -\mathrm{Im}(n)k = -\frac{\mathrm{Im}\,\chi^{(3)}}{2\varepsilon_0 c n_0^2} \cdot \frac{\omega}{c}$$

(3.13)

The term α is the slope of the linear part of the intensity dependent absorption line. It can be approximated to

$$\alpha \approx \frac{-\alpha_0}{2 I_{sat}}$$

(3.14)

Combining equations 3.12 and 3.13 results in

$$\mathrm{Im}\,\chi^{(3)} = \frac{\varepsilon_0 c n_0^2 \alpha_0 \lambda}{2\pi I_{sat}}$$

(3.15)

which is the same as equation 3.3.

Once I_{sat} has been determined from the nonlinear least squares fit and α_0 from a low intensity, linear absorption spectrum, it is a simple matter to compute the imaginary part of the third order susceptibility. This was done for all of the samples and the results are tabulated in table 3.1.

The real part of the susceptibility can be measured by placing an aperture in front of the signal detector, as described earlier on in this chapter. It was found that the trace observed in this case did not exhibit increased transmission peaks and decreased transmission valleys, indicative of a refractive index change but was, in fact, identical to the trace obtained with no aperture. This implies that at these wavelengths, that are very close to the surface plasmon resonance frequency, it is the imaginary part of the susceptibility that dominates over the real part. This, of course, comes as no surprise because the real part of the susceptibility is expected to be low in the vicinity of a resonance decreasing to zero at its peak. The imaginary part of the susceptibility,

RESULTS OBTAINED

Sample	Size Å	$\alpha_0(cm^{-1})$ 516nm	$\alpha_0(cm^{-1})$ 522nm	I_{sat} W/cm² 516nm	I_{sat} W/cm² 522nm	$|Im \chi^{(3)}|$ m²V⁻² 516nm	$|Im \chi^{(3)}|$ m²V⁻² 522nm
N	395	5.50	5.74	3.45×10^8	3.45×10^8	1.12×10^{-19}	6.49×10^{-20}
M	392	8.81	9.32	4.70×10^8	1.89×10^8	7.23×10^{-20}	$1.92 \, 10^{-19}$
O	365	6.10	6.29	1.05×10^8	1.10×10^8	2.24×10^{-19}	2.23×10^{-19}
R	326	25.79	26.82	3.18×10^8	2.36×10^8	3.13×10^{-19}	4.43×10^{-19}
S	184	4.67	4.78	8.01×10^7	3.75×10^8	2.25×10^{-20}	4.97×10^{-20}
Y	179	9.84	9.91	1.93×10^8	1.52×10^8	1.97×10^{-19}	2.54×10^{-19}
K	172	15.94	15.98	2.72×10^8	1.86×10^8	2.26×10^{-19}	3.35×10^{-19}
Z	164	4.69	4.75	1.63×10^8	1.81×10^8	1.11×10^{-19}	1.02×10^{-19}
P	52	8.69	8.82	5.32×10^8	7.13×10^8	6.3×10^{-20}	4.82×10^{-20}
Q	47	8.81	9.09	2.78×10^8	1.40×10^8	1.22×10^{-19}	2.53×10^{-19}

Table 3.1 : Experimental Results

By observation of the table it is obvious that there is no relationship between the size of the inclusions and the nonlinearity of the solution. What *is* evident is that $Im \chi^{(3)}$ is proportional to the square of the absorption coefficient. This result, at a wavelength of 522nm, is shown in figure 3.3.
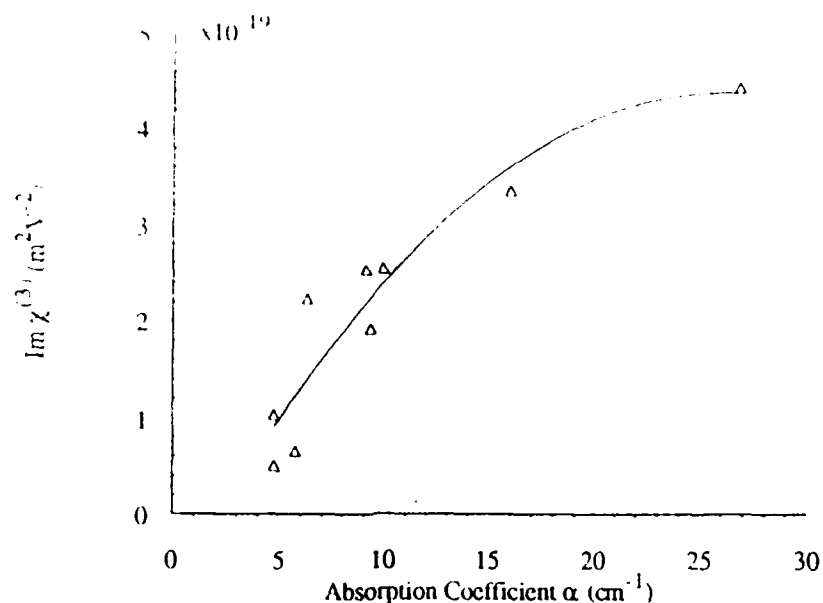
Figure 3.3 : $\text{Im}\,\chi^{(3)}$ Vs α_0. $\lambda = 522nm$.

At higher concentration, the value for $\text{Im}\,\chi^{(3)}$ seems to level off. Past a certain volume fraction of particles, the Maxwell Garnett approximation for calculating the local field in the inclusions is invalidated. If the particles are sufficiently close to interact significantly with each other, the field in each individual one is reduced, leading to a correspondingly lower value for the macroscopic susceptibility.

The quantity, $\text{Im}\,\chi^{(3)}$, in the above table and graph, refers to the nonlinearity of the solution, not that of the actual gold particles. In order to extrapolate, from this, the correct value for the inclusions, the concentration of the solutions and the local field factor discussed in chapter 2 have to be taken into account.

From equation 2.42 it can be seen that the susceptibility for the inclusions, $\chi_i^{(3)}$, is related to the macroscopic susceptibility of the solution through :

$$\chi_i^{(3)} = \frac{\chi^{(3)}}{p|f_1|^2 f_1^2} \tag{3.16}$$

where p is the volume fraction of the inclusions and f_1 is the local field factor. Using this equation it is possible to calculate $\chi_i^{(3)}$ and the results are tabulated in table 3.2.

Sample (Å)	$\text{Im}\,\chi^{(3)}$ 516nm m^2V^{-2}	$\text{Im}\,\chi^{(3)}$ 522nm m^2V^{-2}	P $\times 10^{-5}$	f_1 516nm	f_1 522nm	$\chi_i^{(3)}$ 516nm m^2V^{-2}	$\chi_i^{(3)}$ 522nm m^2V^{-2}
N(395)	-1.12×10^{-19}	-6.49×10^{-20}	1.90	0.992	1.090	6.06×10^{-15}	2.41×10^{-15}
M(392)	-7.23×10^{-0}	-1.92×10^{-19}	3.16	0.964	1.060	2.65×10^{-15}	4.81×10^{-15}
O(365)	-2.24×10^{-19}	-2.23×10^{-19}	2.23	0.937	1.031	1.31×10^{-14}	8.88×10^{-15}
R(326)	-3.13×10^{-19}	-4.43×10^{-19}	9.98	0.886	0.975	5.09×10^{-15}	4.91×10^{-15}
S(184)	-2.25×10^{-20}	-4.97×10^{-20}	1.14	1.114	1.222	1.28×10^{-15}	1.95×10^{-15}
Y(179)	-1.97×10^{-19}	-2.54×10^{-19}	2.65	1.257	1.378	2.97×10^{-15}	2.66×10^{-15}
K(172)	-2.26×10^{-19}	-3.35×10^{-19}	4.37	1.230	1.350	2.26×10^{-15}	2.11×10^{-15}
Z(164)	-1.11×10^{-19}	-1.02×10^{-19}	1.28	1.247	1.367	3.59×10^{-15}	2.29×10^{-15}
P(52)	-6.30×10^{-20}	-4.82×10^{-20}	3.13	0.942	1.036	2.56×10^{-15}	1.34×10^{-15}
Q(47)	-1.22×10^{-19}	-2.53×10^{-19}	2.77	1.085	1.191	3.17×10^{-15}	4.53×10^{-15}

Table 3.2 : Values of $\chi_i^{(3)}$ calculated from the macroscopic susceptibility of the solution.

CONCLUSIONS

The most important conclusion to be drawn from these results is that $\chi_i^{(3)}$ is also independent of the size of the particle, at least within the size range of this study. The values obtained for $\chi_i^{(3)}$ are almost an order of magnitude higher than those obtained by Hache et al.[7, 8, 9] This is not surprising since they calculated their local field factor by comparing the absorption spectrum of their largest particle, which they approximated to have bulk values, to the absorption spectrum of all the other particles, to obtain ε_i, while in this study, the absorption spectrum of the particles was compared to an actual bulk gold spectrum, to calculate ε_i.[10] The latter method yields a lower value for the local field factor and hence a higher valve for the intrinsic susceptibility of the inclusions. By way of comparison, it is interesting to note that BiI_3 microcluster colloidal solutions are reported to have $\chi_i^{(3)}$ values almost two orders of magnitude greater than these ones for gold clusters.[6]

If, within experimental error $\chi_i^{(3)}$ can be taken to be constant, it turns out that the susceptibility of the solution is proportional to the fourth power of the local field factor which is in turn proportional to the square of the absorption coefficient. This is exactly the same as the result expressed in figure 3.3.

In conclusion, using a simple but effective single beam method, it is possible to evaluate the sign and magnitude of both the real and imaginary parts of the nonlinear

susceptibility of a material. It is also possible to determine whether the material is homogeneously or inhomogeneously broadened. The inhomogenously broadened colloidal gold solutions used in this study showed a nonlinear response dominated by the imaginary part of the susceptibility, which is to expected since the experiments were performed in the vicinity of the surface plasmon resonance frequency. The effective or macroscopic nonlinearity of the solution is negative. This is implied by the fact that the absorption decreases with increasing intensity. The nonlinearity of the inclusions is related to the nonlinearity of the solution through the local field factor f_1. At these wavelengths, f_1^2 is nearly real and negative which leads to the conclusion that $\chi_i^{(3)}$ is nearly imaginary and positive. Thus, while the absorption of the colloidal solution decreases with intensity, the absorption of the inclusions actually increases! This is a consequence of the local field correction.

Despite the fact that saturated absorption spectroscopy is a very powerful and useful technique, it provides no information on the dynamics of the interaction between the nonlinear material and the electromagnetic light field. To do this at least two or more beams are required. The following three chapters describe different experimental techniques in which this is done.

REFERENCES

3.1   Sheik-bahae, M., Said, A. A. and van Stryland, E. W. (1989) *High Sensitivity, Single Beam n_2 Measurements*, Opt. Lett. **14**, 955

3.2   Sheik-bahae, M., Said, A. A., Wei, T. H., Hagan, D.J. and van Stryland, E. W. (1990) *Sensitive Measurement of Optical Nonlinearities using a Single Beam*, IEEE J. Quant. Elec. **26**, 760

3.3   Winter, C. S., Oliver, S. N. and Rush, J. D. (1989) *Measurement of the nonlinear refractive index of some metallocenes by the optical power limiter technique*, in Nonlinear Optical Effects in Organic Polymers, eds. Messier, J. *et al*, 247

3.4   Perry, J. W., Khundkar, L. R., Coulter, D. R., Alvarez Jr., D., Marder, S. R., Wei, T. H., Van Stryland, E. W. and Hagan, D. J., ( ) *Excited State Absorption and Optical Limiting in Solutions of Metallopthalocyanines*, in Organic molecules for Nonlinear Optics and Photonics, eds. Messier, J., Kajzar, F. and Prasad, P., NATO ASI series, 369

3.5   Schwerzer, R.E., Kurmer, J. P., Wood, V. E. and Jenkins, J. A. (1990) *Nonlinear Optical Properties of colloidal "Quantum Dot" Composite Materials with Tailored Organic Coatings*, in SPIE Vol. 1337 Nonlinear Optical Properties of Organic Materials III, 132

3.6   Ko, D. K., Lee, J. H. and Chang, J. S. (1992) *Optical bleaching effects in BiI_3 Microcluster Colloid by Saturated Absorption Spectroscopy*, J. Opt. Soc. Am. B **9**, 203

3.7   Hache, F., Ricard, D., Flytzanis, C. and Kreibig, U. (1988) *The Optical Kerr Effect in Small Metal Particles and Metal Colloids : The Case of Gold*, Appl. Phys. A **47**, 347

3.8   Hache, F., Ricard, D. and Flytzanis, C. (1986) *Optical Nonlinearities of Small Metal Particles : Surface Mediated Resonance and Quantum Size Effects*, J. Opt. Soc. Am. B **3**, 1647

3.9   Hache, F., Ricard, D. and Flytzanis, C. (1989) *The Optical Kerr Effect in Small Metal Particles and Metal Doped Glasses: The Case of Gold*, in SPIE Vol. 1127 Nonlinear Optical materials II, ed. Grun, J-B, 115

3.10   Johnson, P. B. and Christy, R. W. (1972) *Optical Constants of the Noble Metals*, Phys. Rev. B **6**, 4370

CHAPTER 4

DEGENERATE FOUR WAVE MIXING USING A COHERENT LIGHT SOURCE

Four wave mixing is one of the most interesting and thoroughly investigated nonlinear optical effects.[1] It is a process that is allowed in all media and has therefore found numerous important applications. Because of the inherent resonant enhancement feature, it has attracted a great deal of attention as a modern spectroscopic technique. With appropriate arrangements four wave mixing can be used to study transitions between excited states, to measure longitudinal and transverse relaxation time etc. Thus, experiments on transient four wave mixing can be used to study not only the particular time-ordered four wave mixing process itself, but also to obtain the various relaxation rates in the medium.

In general, transient four wave mixing deals with the situation where three input pulsed fields, of either the same or different frequencies, interact in a medium in a given time order. The radiative output, which is the fourth wave, shows a time variation depending on the time sequence and separation of the input pulses. If the four waves are all at the same frequency, ω, the interaction is termed degenerate four wave mixing, hereafter called DFWM. In general, two of the fields are strong and are called the pump fields and the weaker third field is called the probe field.

The second nonlinear polarisation term in equation 1.1, which expresses the relationship between polarisation and the applied field,

$$P = \varepsilon_0(\chi^{(1)}E + \chi^{(2)}E^2 + \chi^{(3)}E^3 + \ldots\ldots)$$

(4.1)

i.e., $P = \varepsilon_0\chi^{(3)}E.E.E$ is the one responsible for this process. (Recall that for centrosymmetric or non-isotropic materials $\chi^{(2)} = 0$).

If the two pump beams are counter propagating and the probe beam enters at a small angle with respect to them, as shown in figure 4.1, the signal beam propagates backwards through the medium and remains everywhere a phase conjugate replica of the probe beam. This process is called "Phase Conjugation". It is technologically very important because it is possible to use it to design self-adaptive optical systems that compensate for time varying phase distortions in, for example, high gain laser oscillators and amplifiers, optical fibres, etc.[2]
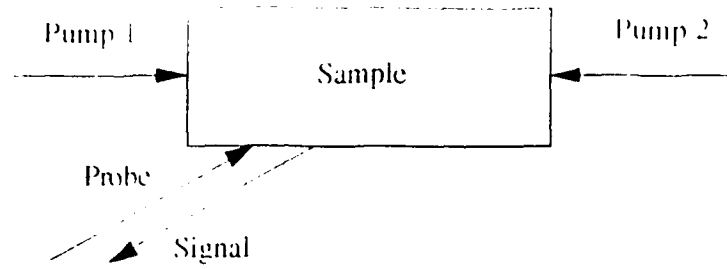
53

Figure 4.1 : Schematic diagram of a phase conjugation experimental set-up.

The first observations of phase conjugation by four wave mixing were reported by Bloom and Bjorkland[3] and Jensen and Hellwarth[4], both parties using CS_2 as the nonlinear medium.

THEORETICAL FORMALISM

The fields involved in the interaction can be described as plane waves using[5]:

$$E_i(r,t) = \frac{1}{2}\left\{A_i(r_i)\exp[i(k_i r - \omega t)] + c.c.\right\}$$ (4.2)

where k_i is the complex propagation vector, r_i is the distance along k_i and c.c. denotes the complex conjugate. k_i can be described as

$$k_i = \hat{k}_i\left(k_i' + i\alpha/2\right)$$ (4.3)

where $\hat{k}_i$ is a unit vector in the direction of propagation of E_i, α is the intensity absorption coefficient in the medium at the frequency ω and $k_i' = \frac{n\omega}{c}$.

The induced nonlinear polarisation can similarly be written as :

$$P^{NL}(r,t) = \frac{1}{2}\left\{P(r)\exp[-i\omega t] + c.c.\right\}$$ (4.4)

Where,

$$P(r)_i = \frac{3}{4}\varepsilon_0\sum_{jkl}\left\{\chi^{(3)}_{ijkl}(-\omega,\omega,\omega,-\omega):A_1(r_1)_j A_2(r_2)_k A_3^*(r_3)_l \exp\left[ir.\left(k_1 + k_2 - k_3^*\right)\right]\right\}$$ (4.5)

By substituting for P^{NL} in the inhomogenous wave equation,

$$\nabla^2 E - \mu_0 \varepsilon \frac{\partial^2 E}{\partial t^2} = \mu_0 \frac{\partial^2 P^N}{\partial t^2} \qquad (4.6)$$

and applying the slowly varying envelope approximation (SVEA) i.e.,

$$k^2 A_i \gg k \frac{\partial A_i}{\partial z} \gg \frac{\partial^2 A_i}{\partial z^2} \qquad (4.7)$$

it is possible to solve for the field amplitudes A_4 and A_3^* which represent the new "signal" beam and the probe beam respectively. By standard techniques, the following equations are obtained,

$$\frac{dA_4}{dz} = iQA_3^* \exp(-\alpha z) \qquad (4.8)$$

$$\frac{dA_3^*}{dz} = iQA_4 \exp(\alpha z) \qquad (4.9)$$

The coupling constant Q is given by

$$Q = \frac{-3\omega}{8cn} \chi^{(3)} A_1(0) A_2(L) \exp\left[-\frac{1}{2}\alpha L\right] \qquad (4.10)$$

where n is the complex index of refraction and $L' = \dfrac{L}{(\hat{k}_1 . \hat{Z})}$, where L is the sample thickness.

Using the boundary conditions $A_4(L) = 0$ (no phase conjugate wave initially) and $A_3^*(0) = A_3^*$ (the initial value of the probe field), the solutions of equations 4.8 and 4.9 are[5],

$$A_4(Z) = \frac{2iQA_3^* \sin[H(Z-L)/2]\exp(-\alpha Z/2)}{\alpha \sin(HL/2) + H\cos(HL/2)} \qquad (4.11)$$

$$A_3^*(Z) = \frac{-A_3^*\{\alpha \sin[H(Z-L)/2] - H\cos[H(Z-L)/2]\}\exp(\alpha Z/2)}{\alpha \sin(HL/2) + H\cos(HL/2)} \qquad (4.12)$$

with,

$$H = \left[4|Q|^2 - \alpha^2\right]^{1/2} \qquad (4.13)$$

The phase conjugate reflectivity is defined as the ratio of the intensity of the generated signal beam to that of the probe beam. It is given by,

$$R = \left| \frac{A_s(0)}{A_4^*(0)} \right|^2 = \left| \frac{2Q\sin(HL/2)}{\alpha\sin(HL/2) + H\cos(HL/2)} \right|^2 \qquad (4.14)$$

In the limit of low reflectivity,

$$R \approx \frac{|Q|^2}{\alpha^2}\left[1 - \exp(-\alpha L)\right]^2 \qquad (4.15)$$

The third order susceptibility, $\chi^{(3)}$, is related to the reflectivity, R through[5, 6, 7] :

$$\chi^{(3)} = \frac{4c^2 n^2 \varepsilon_0 \alpha \sqrt{R}}{3\omega l \sqrt{T}(1-T)} \qquad (4.16)$$

where is α the linear absorption of the sample, and T is the transmission through it.

EXPERIMENT

Phase conjugation is only one of the many different geometrical configurations for DFWM. Another arrangement that is commonly used is called the "folded boxcar" configuration.[8, 9] It was the one used in this study and is shown in figure 4.2. It consists of two pump beams that overlap and interfere in the sample to produce an intensity modulation that is subsequently detected by a probe beam. This intensity modulation can affect the sample in many different ways : it can result in a refractive index modulation, a population modulation, absorptive index modulation etc. The modulation can be visualised as a diffraction grating within the sample. i.e., the pump beams "write" a grating. "Reading" this grating can give information on different physical properties of the medium. This is done by the weak probe beam. When the probe beam is incident on the grating it diffracts in a new direction giving rise to the signal beam. The signal beam is detected by a calibrated photodiode/lock-in-amplifier (LIA) combination. The LIA is triggered by a mechanical chopper in one of the incident beam paths.
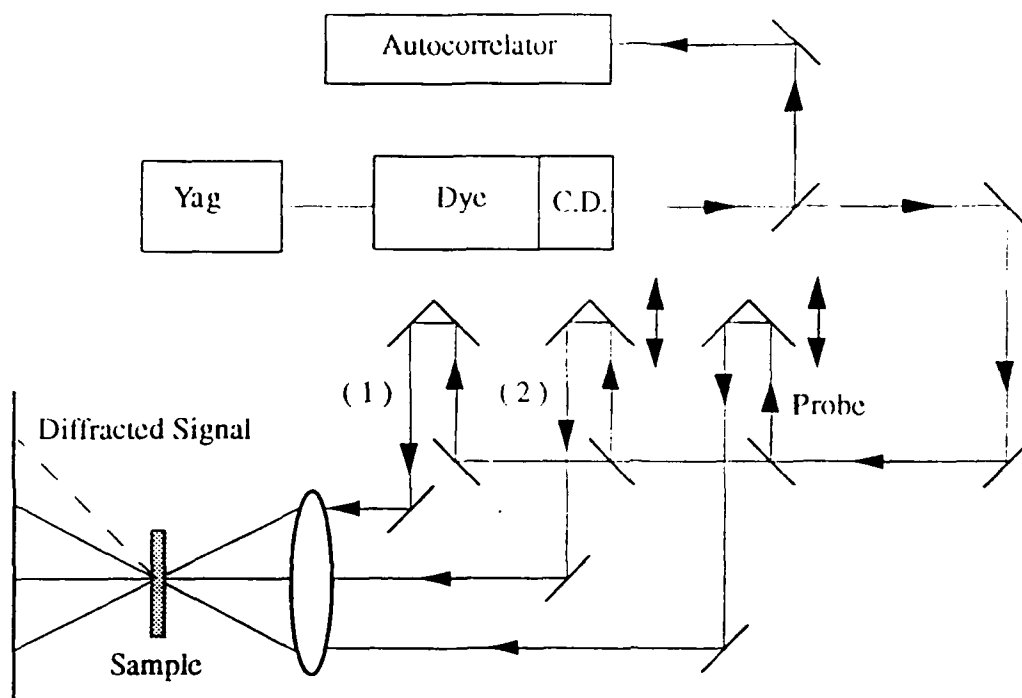
56

Figure 4.2 : DFWM using the "folded boxcar" configuration. (C.D. : Cavity Dumper)

It is now usual to talk about the *diffraction efficiency* which is defined in the same manner as the phase conjugate reflectivity.

The relationship between $\chi^{(3)}$ and the diffraction efficiency η is given by

$$\chi^{(3)} = \frac{8c^2 n^2 \varepsilon_0 \alpha \sqrt{\eta}}{3\omega l \sqrt{T}(1-T)} \tag{4.17}$$

Thus, in order to determine the third order susceptibility of a particular sample one need only measure the ratio of the energy of the diffracted beam to that of the probe beam. It is possible to separate out the different tensorial components of $\chi^{(3)}$ by varying the polarisations for the pump and probe beams. By introducing a time delay between the probe beam and either of the two pump beams it is possible to determine the relaxation time associated with the grating and hence the decay time of the physical property that was modulated by the interference pattern of the pump beams.

The laser system used in this study was a cw mode locked Nd^{3+} doped YAG laser operating at a repetition rate of 100MHz. The output of the laser was frequency doubled and then used to synchronously pump a dye laser. The dye used was Rhodamine 6G which provided a tunability from 560 - 610nm. The output from the dye laser was fed into a cavity dumper in order to reduce the repetition rate. It was possible to vary the repetition rate from 100MHz down to about 40KHz. The width of

the dye laser pulse was measured by autocorrelation techniques using a second harmonic generating crystal and found to be ≈5ps. A cross correlation of the two pump beams was taken at the sample to ensure that they arrived at that point simultaneously. The delay of the probe beam was then scanned to find which setting produced the maximum signal.

Even at the lowest repetition rate of 40 KHz the only sample that it was possible to do measurements on was a 50Å gold colloid dissolved in acetone.

The sample was examined at a range of different repetition rates at a wavelength of 580nm. The concentration was the same in all cases. The results are plotted in figure 4.3. The background at $\tau < 0$ is just scatter from the chopped beam that is collected by the signal detector. This is verified by blocking the other two incident beams. From the figure it can be seen that as the repetition rate is increased, the signal decays with a continuously slower relaxation time. This is indicative of a thermal build-up in the solvent due to absorption of energy by the solute. For the water soluble colloids, the thermal build is more drastic making it impossible to perform any meaningful time resolved experiments, even at the lowest repetition rate of the laser.

When all the three input beams are time coincident at the sample, the magnitude of the DFWM signal is related to $\left|\chi^{(3)}\right|^2$. It can be determined by measuring the diffraction efficiency of the sample, relative to that of a well characterised solvent. This is done to allow for variations in the beam quality. The solvent in this case was CS_2 which has a $\chi^{(3)}_{xxxx}$ value of 6.8×10^{-13} esu.[10] The tensorial component $\chi^{(3)}_{xxxx}$ refers to the case when all three beams are linearly polarised in the same direction, which corresponds to the experimental situation.

When the measurements are done relative to a reference sample, $\chi^{(3)}$ for the test material is obtained using the formula,

$$\chi^{(3)} = \chi^{(3)}_{CS_2} \sqrt{\frac{I}{I_{CS_2}} \frac{n^2}{n^2_{CS_2}}} d_{CS_2} \frac{\alpha \exp(\alpha d / 2)}{1 - \exp(-\alpha d)} \tag{4.18}$$

where, I and I_{CS_2} are the diffraction efficiencies and n and n_{CS_2} are the linear refractive indices for the sample and for the reference material, CS_2, respectively, and α is the linear absorption coefficient of the sample.

Figure 4.3
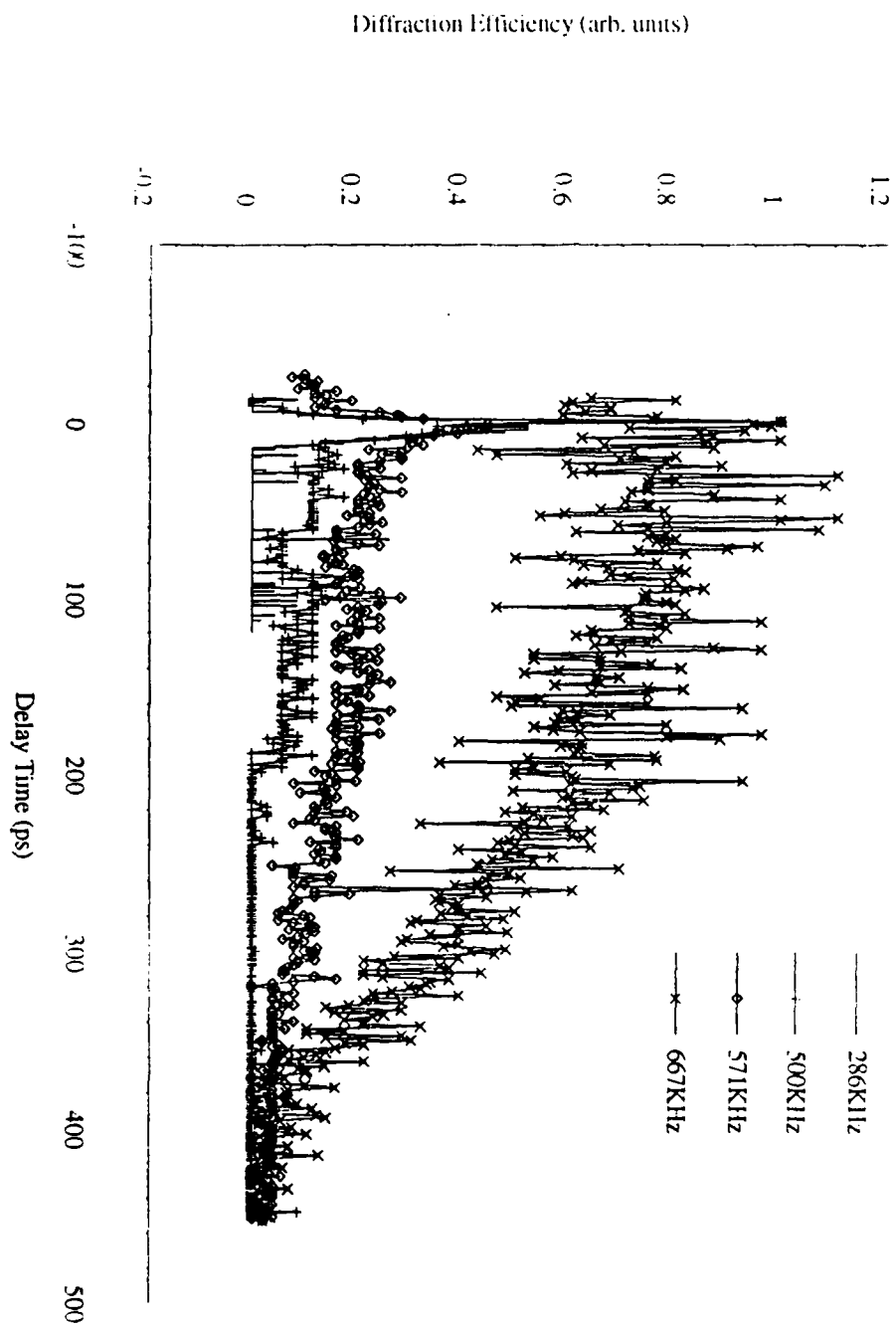
RESULTS OBTAINED

It is possible to examine the relationship between the absorption coefficient and susceptibility by performing the experiment at a range of different wavelengths. The wavelength was varied from 562-606nm, and the results obtained are shown in Table 4.1.

Wavelength (nm)	Absorption Coefficient (cm^{-1})	$\chi^{(3)}(m^2V^{-2})$
562	50.19	1.62×10^{-19}
569	46.04	1.29×10^{-19}
575	42.72	1.00×10^{-19}
581	39.28	8.67×10^{-20}
587	36.48	6.95×10^{-20}
594	32.95	4.58×10^{-20}
600	30.46	3.53×10^{-20}
606	28.21	3.24×10^{-20}

Table 4.1 : Results obtained for wavelength dependent measurements

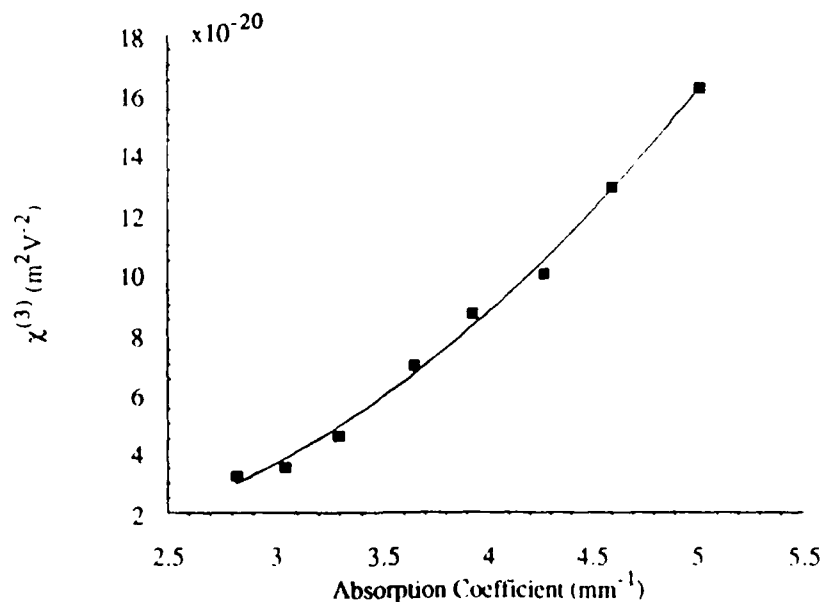The results are shown graphically in figure 4.4.

Figure 4.4 : $\chi^{(3)}$ Vs Absorption Coefficient, α

As expected, $\chi^{(3)}$ is again proportional to the square of the absorption coefficient. The tailing off of $\chi^{(3)}$ with increasing absorption coefficient, as observed in chapter 3, is

not seen here as the concentration is well below the threshold value for the Maxwell Garnett approximation, for the local field in the inclusions, to be applicable. Furthermore, the absorption is changed, not by varying the concentration, but by varying the wavelength.

The value for $\chi_i^{(3)}$, the susceptibility of the inclusions is obtained from the macroscopic susceptibility using the formula 2.42,

$$\chi_i^{(3)} = \frac{\chi^{(3)}}{p|f_1|^2 f_1^2} \qquad (4.19)$$

The results are tabulated in table 4.2.

$|\chi^{(3)}|(m^2 V^{-2})$	f_1	$|\chi_i^{(3)}|(m^2 V^{-2})$
1.62×10^{-19}	1.183	4.02×10^{-16}
1.29×10^{-19}	1.138	3.74×10^{-16}
1.00×10^{-19}	1.092	3.42×10^{-16}
8.67×10^{-20}	1.040	3.60×10^{-16}
6.95×10^{-20}	0.990	3.52×10^{-16}
4.58×10^{-20}	0.928	3.00×10^{-16}
3.53×10^{-20}	0.877	2.90×10^{-16}
3.24×10^{-20}	0.828	3.35×10^{-16}

Table 4.2 : values for the susceptibility of the inclusions, taking into account the local field factor, f_1. The value for p is 2.1×10^{-5}.

CONCLUSIONS

These results imply that the susceptibility of the inclusions is independent of the wavelength or the absorption coefficient of the colloidal solution. The only quantity that varies with wavelength is the local field factor f_1. From equation 2.y it can be seen that the absorption coefficient, α, is directly proportional to the square of the local field factor. Since $\chi^{(3)}$ is proportional to the local field factor to the fourth power, (taking p and $\chi_i^{(3)}$ to be constant, within experimental error), it should also be proportional to the square of the absorption coefficient. This is the result shown in figure 4.4. The values obtained for $\chi_i^{(3)}$ in the wavelength range 562-606nm are of the same order of magnitude as those obtained by Hache et al. at resonance.[11, 12, 13] The reason for this, as explained in chapter 3, lies in the value of the local field factor and the method that is used to determine it.

The values in the above table are absolute since, in this experimental arrangement, there is no way of determining the sign of χ. It is also not possible to say what contribution of the diffracted signal comes from the real part of the susceptibility and what contribution comes from the imaginary part. The local field factor f, at these wavelengths has real and imaginary parts of equal magnitude, both being positive. This information is, however, redundant since the magnitudes of the real and imaginary parts of the macroscopic susceptibility are unknown. This means that the relative magnitudes of the real and imaginary parts of the susceptibility of the inclusions also remains unknown. The only thing that can be said is that the real part of the susceptibility is probably not negligible. This was the case in Chapter 3 (i.e., the real part of the susceptibility was negligible)where the experiments were being performed very close to the surface plasmon resonance frequency. As explained in Chapter 3, the further away from resonance that the experiments are performed, the greater should be the relative contribution of the real part of the susceptibility.

The change in the DFWM signal as a function of time delay of the probe beam gives the decay of the grating and hence the time response of the optical nonlinearity. The experiments were all performed at a repetition rate of 286 Hz. The response time in each case, which is a higher order autocorrelation of the laser pulses convoluted with the material response, was found to be shorter than the intensity autocorrelation width, indicating that the experimental resolution is limited by the laser pulse width. The only information to be gleaned from this experiment, therefore, is that the lifetime of the excited state in the resonant two level system is *at most* 5ps. This result is consistent with measurements performed by Hache *et al*,[11, 12, 13] Bloemer *et al*[14] and Heilweil and Hochstrasser.[15] A similar result was found by yang *et al* for Copper nanocluster colloidal solutions.[16]

The relaxation processes in a resonant two level system are usually described by a second parameter, T_2 along with the lifetime of the excited state. T_1, also known as the longitudinal relaxation time. The parameter T_2 is known as the transverse relaxation time or the phase relaxation time . It represents the decay of the coherence between the two levels. By an appropriate arrangement it is possible to determine T_2 from the above DFWM experiment as well. However, T_2 generally lies in the fsec time regime and so, using coherent 5 psec pulses would give very little information about it. The following chapter describes a novel technique for determining T_2 using incoherent light.

REFERENCES

4.1   Bloembergen, N. (1979), in *Laser Spectroscopy* IV, eds. Walther, H. and Rothe, K. W. (Springer, Berlin), 340

4.2   Eichler, H.J., Günter, P. and Pohl, D.W. (1986) in *laser-induced dynamic gratings*, Springer Series in Optical Sciences.

4.3   Bloom, D. M., and Bjorkland, G.E. (1977), *Conjugate wavefront generation and image reconstruction by four wave mixing*, Appl. Phys. Lett **31**, 592

4.4   Jensen, S. L. and Hellwarth, R.W. (1978), *Observation of the time reversed replica of a monochromatic optical wave*, Appl. Phys. Lett **32**, 166

4.5   Caro, R. G. and Gower, M. C. (1982) *Phase Conjugation by Degenerate Four-Wave Mixing in Absorbing Media*, IEEE J. Quant. Elec. **QE-18**, 1376

4.6   Gower, M. C. (1985) *Diagrammatical Analysis of Phase Conjugation using Four- and Three-Wave Mixing Processes in Kerr-Like Nonsaturated Media*, IEEE J. Quant. Elec., **QE-21**, 182

4.7   Pepper, D. M. and Yariv, A. (1983) in *Optical Phase Conjugation*, ed. Fisher, R. A., Academic Press, London, 23

4.8   Shirley, J. A., Hall, R. J., and Eckbeth, A.C. (1980), *Folded BOXCARS for Rotational Raman Studies*, Opt. Lett. **5**, 380

4.9   Bogdan, A.R., Prior, Y. and Bloembergen, N., (1981), *Pressure-Induced Degenerate Frequency Resonance in Four-Wave Light Mixing*, Opt. Lett. **6**, 82

4.10   Xuan, N.P., Ferrier, J. L., Gazengel, J. and Rivoire, G. (1984) Opt. Commun. **51**, 433

4.11   Hache, F., Ricard, D., Flytzanis, C. and Kreibig, U. (1988) *The Optical Kerr Effect in Small Metal Particles and Metal Colloids : The Case of Gold*, Appl. Phys. A **47**, 347

4.12   Hache, F., Ricard, D. and Flytzanis, C. (1986) *Optical Nonlinearities of Small Metal Particles : Surface Mediated Resonance and Quantum Size Effects*, J. Opt. Soc. Am. B **3**, 1647

4.13   Hache, F., Ricard, D. and Flytzanis, C. (1989) *The Optical Kerr Effect in Small Metal Particles and Metal Doped Glasses: The Case of Gold*, in SPIE Vol. 1127 Nonlinear Optical materials II, ed. Grun, J-B, 115

4.14   Bloemer, M. J., Haus, J. W. and Ashley, P. R. (1990) *Degenerate Four-Wave mixing in Colloidal Gold as a Function of Particle size*, J. Opt. Soc. Am. B **7**, 790

4.15   Heilweil, E. J. and Hochstrasser, R. M. (1985) *Nonlinear Spectroscopy and Picosecond transient Grating Study of Colloidal Gold*, J. Chem. Phys. **82**, 4762

4.16   Yang, L., Becker, K., Smith, F. M., Magruder III, R. H., Haglund, Jr., R. F., Yang, L., Dorsinville, R., Alfano, R. R. and Zuhr, R. A. (1994) *Size Dependence of the Third-order Susceptibility of Copper Nanoclusters Investigated by Four-Wave Mixing*, J. Opt. Soc. Am. B **11**, 457

CHAPTER 5

DEGENERATE FOUR WAVE MIXING USING INCOHERENT LIGHT

In order to understand the dynamical behaviour of light-matter interaction, it is very important to study the relaxation processes associated with the excited states of materials. In many cases of interest, especially in condensed matter, these relaxation processes take place on a subpicosecond or femtosecond timescale. In transient spectroscopy using coherent light, the time resolution of the experiment is limited by the pulse width of the exciting radiation.[1, 2] Thus in order to probe the dynamical behaviour of such materials effectively it is essential to have access to ultrafast lasers. To this end, a lot of effort has been devoted to obtaining short pulse lasers and with CPM dye lasers, pulses with widths of less than 100 fs have been obtained. Even shorter pulses, with pulse widths of 6 fs have been generated by using a pulse compression technique.[3, 4] There are, however, several problems associated with using such short pulses. Firstly, the optics required to generate or compress ultra short pulses are complicated and prohibitively expensive. Also, as there are not very many suitable combinations of laser dye/saturable absorber, ultra short pulses can only be generated in a very limited wavelength regime. Finally, even if one were able to succeed in getting a short enough pulse at a suitable wavelength, there are further problems associated with the dispersion of the pulse as it traverses through the optics of the experiments.

One solution to this problem is to perform the experiments in the frequency domain. In 1978 Yajima et al [5, 6] proposed resonant Rayleigh-type mixing spectroscopy for the measurement of the longitudinal relaxation time, T_1, and the homogenous transverse relaxation time, T_2, and the relaxation times in some materials have actually been measured.[7] However in this case the analysis of the results is extremely complex and can lead to ambiguities in the determination of these times.

Prompted by these difficulties, in 1984, Morita et al [8] and Beach and Hartmann [9] independently came up with a new spectroscopic technique that utilises temporally incoherent light to determine ultrafast relaxation times. Traditionally optical coherent experiments have always been performed with coherent laser light. While this may be essential for experiments such as self induced transparency, it is not a universal requirement. Indeed, not only can optical coherent transients be generated with an

incoherent light source, there are decided advantages in doing so. Optical transitions can only be induced within the bandwidth of the excitation source. For a laser oscillating in, at most, a few well defined modes, this means that only a small fraction of the atoms or molecules within the resonance line participate in an experiment. This problem can be overcome by performing the experiment using a broadband incoherent light source which also provides ultrahigh time resolution. The basis of this method is that the signal light generated or modulated by nonlinear optical effects consists of a correlation of the material response and the input field and, as such, is dependent on the correlation time of the pulse instead of its width. Temporally incoherent light has a wide spectral width, $\Delta\upsilon$, and a correspondingly short correlation time determined by $1/\Delta\upsilon$, which is much shorter than its temporal width. This kind of light appears as a single pulse of duration τ_c in an autocorrelation experiment [10] and is therefore expected to play the same role as a short pulse in experiments utilising the correlation technique. This fact has been verified experimentally in several situations, including Raman spectroscopy,[11, 12, 17, 19] for measuring vibrational relaxation times, and Degenerate four wave mixing (DFWM) [13-19], photon echoes [9, 20] and pump and probe spectroscopy [21] for measuring phase relaxation times and excited state lifetimes of nonlinear materials. This chapter focuses on the measurement of the dephasing time of colloidal gold solutions by DFWM spectroscopy. In the self diffraction configuration, two temporally incoherent light beams with wave vectors $\vec{k}_1$ and $\vec{k}_2$, originating from a single beam at frequency ω are made to overlap in a nonlinear sample.[2] Due to the third order nonlinearity of the material, two new output beams are generated at the same frequency but in the directions $\vec{k}_3 = 2\vec{k}_2 - \vec{k}_1$ and $\vec{k}_4 = 2\vec{k}_1 - \vec{k}_2$. Even if the pulse width of the light is much longer than either T_1 or T_2, the correlation trace, i.e., the diffracted light intensity as a function of delay time, τ, between the two beams, decays exponentially with a time dependent on T_2, provided that the coherence time of the pulse, τ_c, is less than T_2.[8] This fact is extremely useful because it is far easier to prepare an incoherent light source with a short correlation time τ_c than to produce an ultrashort pulse with the same duration, especially in the range less than 1 ps. In an extreme case, even cw light, which has an infinite duration, is capable of providing fs time resolution provided it has the adequate spectral width. In the event that τ_c is not very short, the resolution of the experiment is limited on it.

THEORETICAL BACKGROUND

The electric fields of the incoherent light beams involved in the interaction can be described as [8]

$$E(\vec{r},t) = \xi\left(t - \frac{\vec{n}.\vec{r}}{v}\right)\exp\left(-i\omega t + i\vec{k}.\vec{r}\right) + c.c. \tag{5.1}$$

with,

$$\xi(t) = \varepsilon(t)R(t) \tag{5.2}$$

where $\vec{k}$ is the propagation vector, $\vec{n}$ is a unit vector in the direction of $\vec{k}$, c.c. denotes the complex conjugate, $\varepsilon(t)$ is a normal function and $R(t)$ is a complex random function representing a stochastic stationary Gaussian process, which is how the incoherent beam is represented.

For such a function,

$$\left\langle R^{*}(t)R(t+\tau)\right\rangle = f(\tau) \tag{5.3}$$

$$\left\langle R(t)R(t+\tau)\right\rangle = \left\langle R^{*}(t)R^{*}(t+\tau)\right\rangle = 0 \tag{5.4}$$

$$\left\langle R^{*}(t)\right\rangle = \left\langle R(t)\right\rangle = 0 \tag{5.5}$$

where $f(\tau)$ is the correlation function.

The total electric field incident on the material is a superposition of the two fields with wave vectors $\vec{k}_1$ and $\vec{k}_2$ where the field with wave vector $\vec{k}_2$ is temporally delayed by τ relative to the other. The total field can be written in the form

$$E(\vec{r},t) = E_1 + E_2 = \left\{ \xi\left(t + \tau - \frac{\vec{n}.\vec{r}}{v}\right)\exp\left(-i\omega(t+\tau) + i\vec{k}_1.\vec{r}\right) + \right.$$

$$\left. \xi\left(t - \frac{\vec{n}.\vec{r}}{v}\right)\exp\left(-i\omega t + i\vec{k}_2.\vec{r}\right)\right\} + c.c. \tag{5.6}$$

The relaxation processes in a resonant two level system are usually described by the two parameters, the longitudinal relaxation time, T_1, representing the decay of the population difference and the transverse relaxation time, T_2, representing the decay of

67

the coherence between the two levels. If there is a distribution of transition frequencies between the levels the system is considered to be inhomogenously broadened

The output light field at the frequency, ω, in a four wave mixing process is proportional to the third order induced polarisation,[22] which has the form,

$$P^{(3)}(\vec{r},t) = P^{(3)}(\vec{r},t)\exp(-i\omega t) + c.c.$$ (5.7)

with,

$$P^{(3)}(\vec{r},t) = N\int_{0} d\omega_0 \mu_{ab}\hat{\rho}_{ba}^{(3)}(\vec{r},t,\omega_0)g(\omega_0)$$ (5.8)

where N is the atomic number density, the subscripts a and b denote lower and upper levels, respectively, μ_{ab} is the electric dipole matrix element of the transition between the two levels, and $g(\omega_0)$ is the distribution function of the transition frequency, ω_0, characterising the inhomogenous broadening. $\hat{\rho}_{ba}^{(3)}(\vec{r},t,\omega_0)$ is the third order, off-diagonal density matrix element. It contains four components at the wave vectors $\vec{k}_1$, $\vec{k}_2$, $\vec{k}_3 = 2\vec{k}_2 - \vec{k}_1$, and $\vec{k}_4 = 2\vec{k}_1 - \vec{k}_2$. Since the experiment involves detecting and measuring the signal in the direction $\vec{k}_3$, it is only necessary to consider the $\vec{k}_3$ component of $\hat{\rho}_{ba}^{(3)}$.

This is given by the equation,[8]

$$\hat{\rho}_{ba}^{(3)}(\vec{k}_3) = -2i\rho^{(0)}\left[\frac{\mu}{\hbar}\right]^3 \exp(i\vec{k}_3.\vec{r} + i\omega\tau) X$$

$$\int_{-\infty}^{t} dt_1 \int_{-\infty}^{t_1} dt_2 \int_{-\infty}^{t_2} dt_3 \left\{\xi(t_1)\xi(t_2)\xi^*(t_3 + \tau)\exp\left[-i(\omega_0 - \omega)(t_r - t_1 - t_2 + t_3)\right]\right.$$

$$\left.+\xi(t_1)\xi^*(t_2 + \tau)\xi(t_3)\exp\left[-i(\omega_0 - \omega)(t_r - t_1 + t_2 - t_3)\right]\right\}$$

$$X\exp\left[-\gamma_1(t_1 - t_2) - \gamma_2(t_r - t_1 + t_2 - t_3)\right]$$ (5.9)

where $\gamma_1 = T_1^{-1}$, $\gamma_2 = T_2^{-1}$, $\rho^{(0)}$ is the thermal equilibrium value of the population difference of the two levels, $t_r = t - \dfrac{(\vec{n}.\vec{r})}{v}$ is the reduced time assuming that $n_1 = n_2 = n$ and $\mu_{ba} = \mu_{ab} = \mu$.

The output light intensity, which is the quantity that is actually experimentally measured is proportional to $\left| \hat{P}^{(3)}(\vec{r},t) \right|^2$. However, because of the random nature of $\hat{P}^{(3)}(\vec{r},t)$, it is necessary to calculate the statistically averaged value, $J(\vec{k}_3)$, of this quantity, which can be written as,[8]

$$J(\vec{k}_3) = \left\langle \left| \hat{P}^{(3)}(\vec{r},t) \right|^2 \right\rangle \propto \left| \varepsilon(t_r) \right|^6 F(\tau) \tag{5.10}$$

The function $F(\tau)$ determines the shape of the correlation profile. It can be calculated when a reasonable form is given to the correlation function $f(\tau)$. $f(\tau)$ is usually approximated to be a delta function. Though not absolutely correct, this choice is reasonable since the rate to be measured is much greater than the coherence time of the pulse. In the event that the coherence time is comparable to or greater than the quantity being measured, the analysis is unnecessary since the only information that can be obtained in such a case is, a value for the upper limit of that quantity.

The explicit form of $F(\tau)$ when $g(\omega_0)$ is a Gaussian distribution centred at ω_0 with a width of $\delta\omega$ is shown for two extreme cases in what follows :[8]

(i) Homogenous broadening case, $\delta\omega = 0$.

(i.i) $\tau > 0$

$$F(\tau) = c_1 \left[u + \frac{2(3-4u)}{1-u} \exp(-2x) - 4(1-u)\exp\left[-(2+u)x\right] \right.$$

$$\left. + \frac{u^2(3-u)}{1-u} \exp(-2ux) \right] \tag{5.11}$$

(i.ii) $\tau = 0$

$$F(0) = c_1 \left(2 + 2u + \frac{1}{4}u^2 \right) \tag{5.12}$$

(i.iii) $\tau < 0$

$$F(\tau) = c_1 \left[u + 2\exp(2x) \right] \tag{5.13}$$

(ii) Extremely inhomogenous broadening case, $\delta\omega \to \infty$

(ii.i) $\tau > 0$

$$F(\tau) = c_2 \left[u + \frac{32(1-u)^3 \exp(-4x) + 32(1-u)\exp\left[-(2+u)x\right] + 8u \exp(-2ux)}{(2-u)^3} \right]$$

<div align="right">(5.14)</div>

(ii.ii) $\tau = 0$

$$F(0) = c_2(u + 4)$$

<div align="right">(5.15)</div>

(ii.iii) $\tau < 0$

$$F(\tau) = c_2 u$$

<div align="right">(5.16)</div>

where,

$$c_1 = \frac{D^3}{4\gamma_1\gamma_2}$$

<div align="right">(5.17)</div>

and

$$c_2 = \frac{\sqrt{2\pi}D^3}{8\gamma_1^2\delta\omega}$$

<div align="right">(5.18)</div>

$u = \dfrac{\gamma_1}{\gamma_2}$, $x = \gamma_2\tau$ and D is a positive constant proportional to the spectral density of the light.

COMPARISON WITH SIMILAR EXPERIMENTS USING SHORT PULSES

It is instructive, at this stage, to compare the signal behaviour in this case to that in a conventional, short pulse, two beam self diffraction experiment, hereafter referred to as short pulse DFWM. The similarity between the processes lies in the fact that both profiles reflect the relaxation processes governed dominantly by the phase relaxation time T_2. There are, however, three main differences.

(i) The correlation traces in this experiment do not necessarily decay as single exponentials, while those of short pulse DFWM experiments always decay single exponentially at a rate proportional to $\dfrac{1}{T_2}$.

(ii) The present correlation profiles have non zero values at $\tau = \pm\infty$, while no background exists in the short pulse DFWM case.

(iii) In this experiment the correlation profiles at $\tau < 0$ grow up with increasing τ in the homogenous broadening case, while those in the short pulse DFWM case are always zero at $\tau < 0$.

From (i) it can be seen that the profile from such an experiment, thus, does not necessarily give us one of the relaxation times T_1 and T_2 in as unambiguous a manner as the usual self diffraction experiments. If, however, $T_1 >> T_2$, the profiles represent a single exponential decay with the rates $2T_2^{-1}$ and $4T_2^{-1}$ for the homogenous and extremely inhomogenous cases, respectively. These rates are consistent with those in the short pulse case and T_2 can be uniquely determined. In condensed matter, such as singlet-singlet transitions of dye molecules, interband transitions of semiconductors etc., T_2 is generally very short and often falls far below 1ps. In these transitions, the population relaxation time T_1 is often much longer than T_2. Therefore, in these cases the present method is a powerful tool for determining T_2.

In the event that T_1 is not much longer than T_2, the present method cannot determine the relaxation time T_2 definitely. However, even in the worst case, it is possible to determine T_2 within the error factors of 1.5 and 2.7 in the homogenous and extremely inhomogenous broadening cases, respectively.[8]

EXPERIMENTAL SET-UP

The experimental set-up, for measuring T_2, is shown in figure 5.1. The PRA dye laser was pumped by a PRA Nitrogen laser and emitted 500ps pulses with energies of 30 - 40 μJ at a repetition rate of 1 - 5 Hz. The dye used was Coumarin 485.
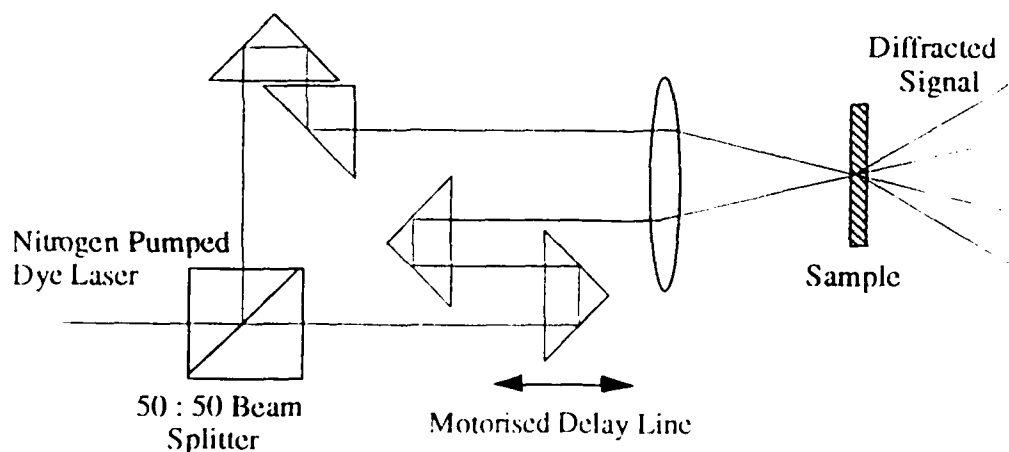

Figure 5.1 : Self diffraction configuration for degenerate four wave mixing.

The output beam was divided into two parts using a 50:50 beam splitter. After passing the two beams through variable and fixed delay lines, they were recombined in the sample (thickness 0.1 mm) using a 20 cm lens. The delay time τ between the beams was changed by a stepping motor.

The spectral width of the emitted radiation was increased by replacing the diffraction grating in the dye laser oscillator cavity with a mirror.[17, 19] Under these conditions the bandwidth was found to be 10.5 nm with a centre wavelength of 522nm. This corresponds to a coherence time of 86.5fs.

Figure 5.2 shows the results of the bandwidth measurement. The experiment was performed by passing the beam through a monochromator and monitoring its energy at the exit slit as a function of the wavelength selected.
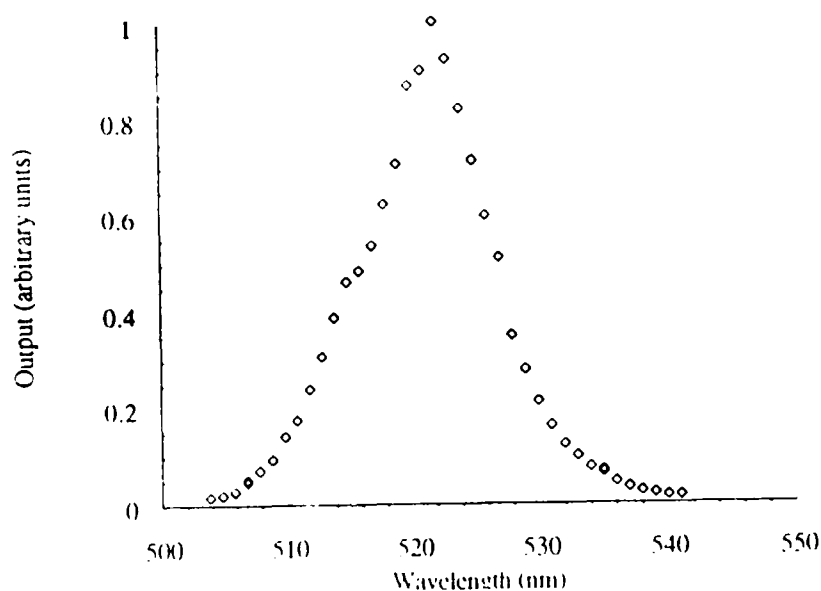

Figure 5.2 : Output intensity Vs λ for measuring the bandwidth of the beam

The samples studied were :

SAMPLE	AVERAGE DIAMETER (Å)
Q	47
C	50
P	52
S	184
O	365
M	392
N	395

RESULTS OBTAINED AND CONCLUSIONS ON THE MEASUREMENT OF THE DEPHASING TIME

The correlation profiles for three of the samples, C, S and M are shown in figures 5.3, 5.4 and 5.5, respectively. These three samples reflect the range of sizes used in this study.
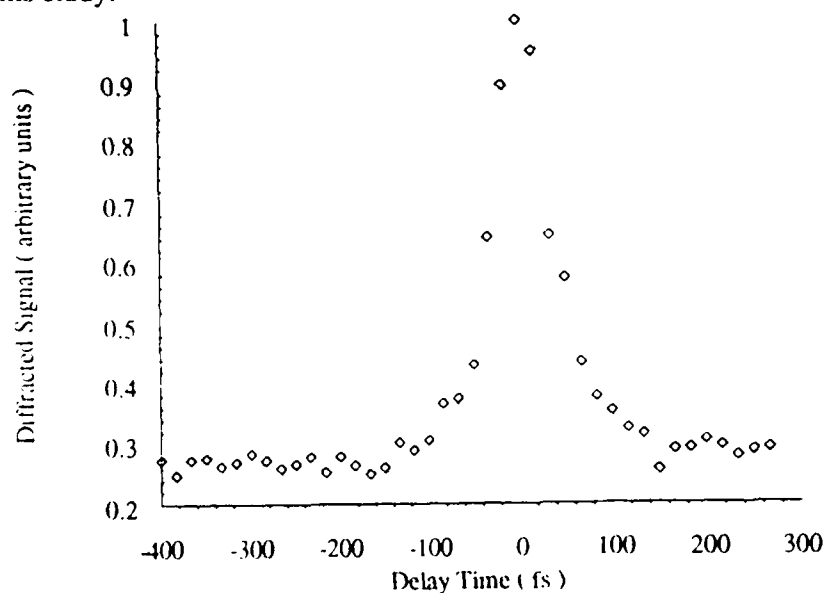
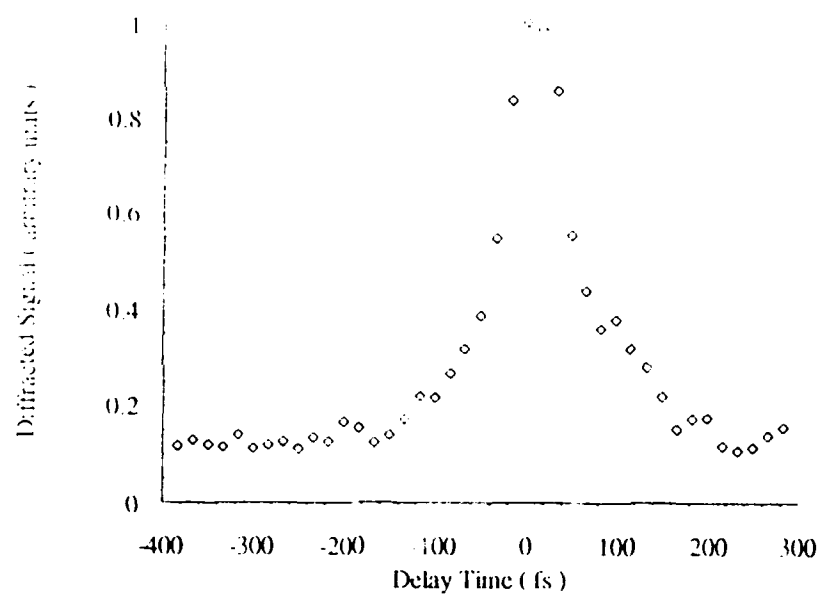Figure 5.3 : Sample C, Diffracted intensity Vs delay time.

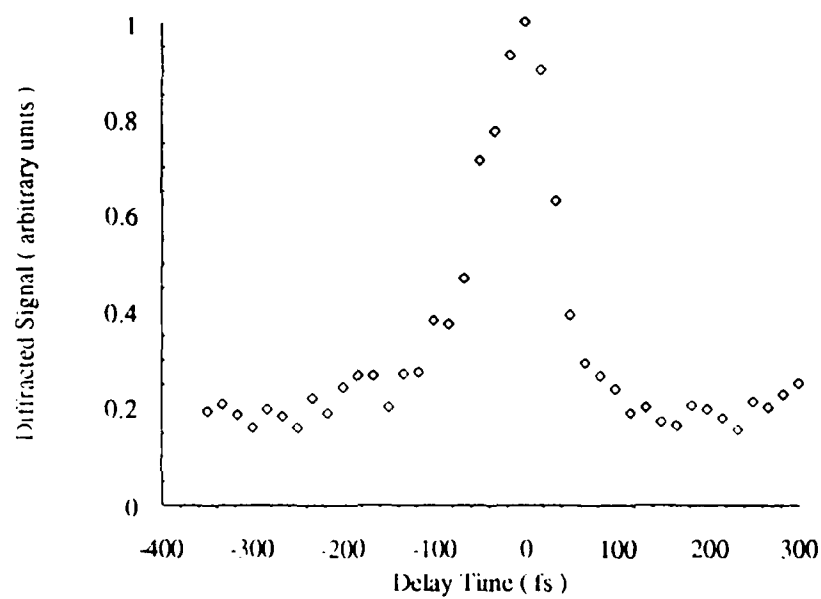Figure 5.4 : Sample S, Diffracted intensity Vs delay time.

Figure 5.5 : Sample M, Diffracted intensity Vs delay time.

The experiment was also performed on a dye solution of Rhodamine B, as a reference material, known to have a sub-ps phase relaxation time.[23] The result is shown in figure 5.6.
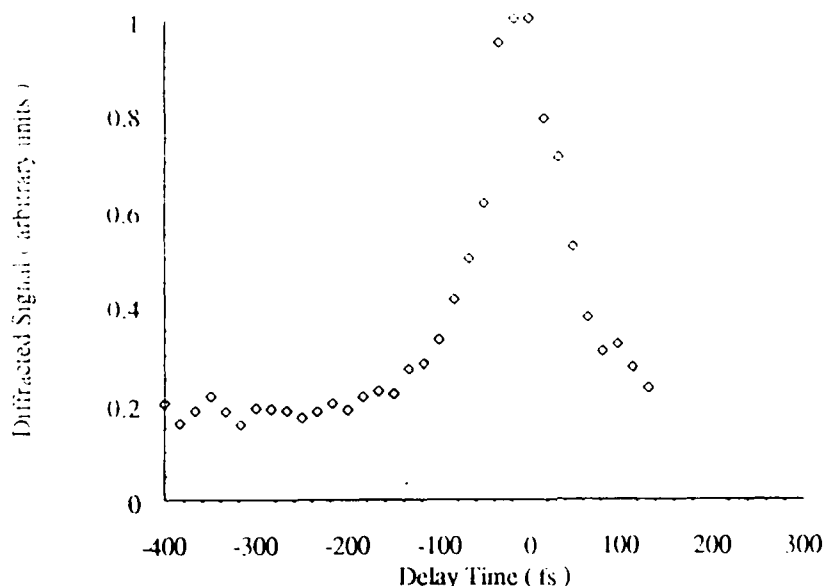
Figure 5.6 : Rhodamine B, Diffracted Intensity Vs delay time.

From all the figures, 5.3 - 5.6, it can be seen that the correlation trace is symmetric about the zero delay position. The background signal at $\tau = \pm\infty$ is also evident. The signal to noise ratio in this region is quite low, hence the apparent fluctuations.

The fact of the correlation trace being symmetric implies that the relaxation time is faster than the coherence time of the pulse, i.e. the resolution of the experiment. The observed signal, therefore gives a correlation profile $|G(\tau)|^2$ of the incident incoherent light where $G(\tau) = \exp(-|\tau|/\tau_c)$ is the autocorrelation function of the incident field. In such cases, however, it is *still* possible to measure T_2 by monitoring both the diffracted beams simultaneously and measuring the time lag between them. For homogeneously broadened systems the two traces should completely overlap. For extremely inhomogenous systems, however, the two traces will be separated in time.[16, 17, 19, 24] This time corresponds to the phase relaxation time. Depending on the degree of the inhomogeniety, however, this time will vary and is, thus, not a completely accurate way of determining T_2.

Nevertheless, the experiment was performed and it was found that the two traces overlapped completely. This could mean one of two things :

(i) The materials can be described as homogenous systems. From Chapter 3, this is known to be untrue.

(ii) The materials can be described as inhomogenous systems but with a phase relaxation time shorter than that which can be measured using the delay line. The delay line moves in 2.5 μm steps and, since it is a double pass line, this corresponds to a time delay of 17fs. This, then, is the ultimate resolution of the experiment. Thus, even if the materials are extremely inhomogenously broadened but have a phase relaxation time of the order of 20 fs, the two correlation traces will not be separated in time.

Point (ii) is taken to be the correct interpretation of the results as it is consistent with the findings of Chapter 3. It is also consistent with theoretical calculations done by Flytzanis et al.[25, 26]

MEASUREMENT OF THE MAGNITUDE OF THE NONLINEAR SUSCEPTIBILITY

By measuring the magnitude of the diffracted signal, when both the beams are time coincident on the sample, it is possible to determine the absolute value of the nonlinear susceptibility $\chi^{(3)}$, using equation 4.17 of chapter 4.

$$\chi^{(3)} = \frac{8c^2 n^2 \varepsilon_0 \alpha \sqrt{\eta}}{3\omega l \sqrt{T}(1-T)} \tag{5.19}$$

The diffraction efficiency is given by the ratio of the diffracted signal to that of one of the pump beams.

Table 5.2 displays the results of the calculations, including the results obtained for the susceptibility of the inclusions using the formula 2.42,

$$\chi_i^{(3)} = \frac{\chi^{(3)}}{p|f_1|^2 f_1^2} \tag{5.20}$$

Sample	Size (Å)	Abs. Coeff. (cm^{-1})	$\chi^{(3)}(m^2 V^{-2})$	f_i	$\chi_i^{(3)}(m^2 V^{-2})$
N	395	221.5	3.23×10^{-19}	1.074	3.31×10^{-16}
M	392	135.6	1.15×10^{-19}	1.064	1.98×10^{-16}
O	365	125.3	1.13×10^{-19}	1.028	2.34×10^{-16}
S	184	153.8	1.90×10^{-19}	1.330	1.48×10^{-16}
P	52	253.3	7.13×10^{-20}	1.003	7.86×10^{-17}
C	50	50.7	4.42×10^{-20}	1.133	1.72×10^{-16}
Q	47	451.1	4.95×10^{-19}	1.118	2.21×10^{-16}

Table 5.2 : Values for the macroscopic susceptibility and the susceptibility of the inclusions, obtained using incoherent light.

$\chi^{(3)}$ again shows the familiar square dependence on the absorption coefficient. This is shown graphically in figure 5.7. The values for $\chi_i^{(3)}$ are of the same order of magnitude as those measured by Hache et al.[27, 28, 29] At first this seems surprising in light of the arguments of Chapter 3. However, bearing in mind that the experiment measures an absolute value for $\chi^{(3)}$, (as opposed to a comparative value) there is scope for error in the measurement, especially in the determination of the intensity. The results obtained could be improved upon by performing the experiment relative to a well characterised sample, such as CS_2 to allow for variations in the beam quality. This, however, was not done as the results were only out by a factor of 2-4, which, in nonlinear optics is generally considered a reasonable error. One conclusion that can be drawn from these results is that the diffracted signal obtained is from a truly electronic effect and not from a thermal grating. The logic behind this conclusion is that if a thermal grating were contributing to the signal, the diffraction efficiency obtained would be orders of magnitude higher.
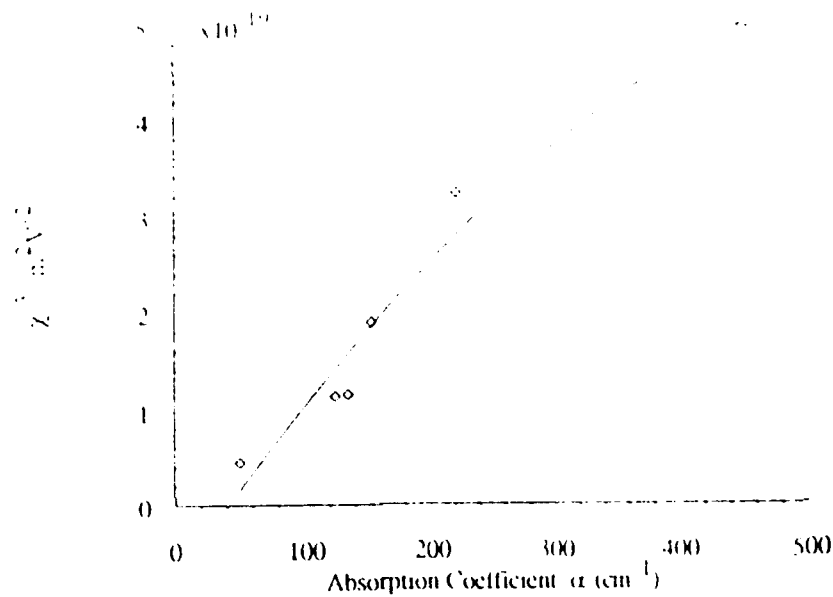
Figure 5.7 : $\chi^{(3)}$ Vs Absorption coefficient

The local field factor, squared, f_i^2, at a wavelength of 522nm is mostly real and negative implying that the macroscopic susceptibility $\chi^{(3)}$, and the susceptibility of the inclusions $\chi_i^{(3)}$, have different signs. However, in this experimental configuration, as in short pulse DFWM, it is not possible to determine the sign of the susceptibility.

CONCLUSIONS

The only conclusions to be drawn from this chapter then are that the samples have a phase relaxation time of the order of or faster than 20 fsec and that the susceptibility of the inclusions is $\equiv 2\times10^{-16}m^2V^{-2}$. In order to determine what mechanisms contribute to the value obtained for $\chi_m^{(3)}$ it is essential to know its sign and, as accurately as possible, its response time. The results obtained from previous chapters and this chapter, though good, are not conclusive and therefore, it is necessary to perform further experiments to evaluate the sign and the temporal response of $\chi_i^{(3)}$. The following chapter describes an experiment that measures the deflection of a beam, due to the optical Kerr effect, passing through a nonlinear material on which an intense pump beam is incident, as a function of time delay between the probing and the pumping beams. The laser used has a fsec pulse width and the temporal resolution is therefore better than that obtained in Chapter 4. It is also possible to determine, from the experiment, the sign of the nonlinearity.

78

REFERENCES

5.1   ULTRASHORT LIGHT PULSES

5.2   Eichler, H.J., Günter, P. and Pohl, D.W. (1986) in *laser-induced dynamic gratings*, Springer Series in Optical Sciences.

5.3   Knox, W.H. Fork, R.L., Downer, M.C., Stolen, R.H. and Shank, C.V., Valdmanis, J. A. (1985) *Optical Pulse Compression to 8fs at a 5KHz Repetition Rate*, Appl. Phys. Lett. **46**, 1120

5.4   Brito-Cruz, C.H., Becker, P. C., Fork, R.L. and Shank, C.V. (1988) *Phase Correction of Femtosecond Optical Pulses using a Combination of Prisms and Gratings*, Opt. lett. **13**, 123

5.5   Yajima, T. and Souma, H. (1978) *Study of Ultrafast Processes by Resonant Rayleigh Type Optical Mixing I. Theory*, Phys Rev A **17**, 309

5.6   Yajima, T., Souma, H. and Ishida, Y. (1978) *Study of Ultrafast Processes by Resonant Rayleigh Type Optical Mixing II. Experiment on Dye Solutions*, Phys Rev A **17**, 324

5.7   Heilweil, E.J. and Hochstrasser, R.M. (1985) *Nonlinear spectroscopy and picosecond transient grating study of colloidal gold*, J. Chem. Phys. **82**, 4762

5.8   Morita, N. and Yajima, T. (1984) *Ultrahigh-time resolution coherent transient spectroscopy with incoherent light*, Phys Rev A **30**, 2525

5.9   Beach, R. and Hartmann, S.R. (1984) *Incoherent Photon Echoes*, Phys. Rev. Lett. **53**, 663

5.10   Ippen, E.P. and Shank, C.V. *Ultrashort light pulses*, ed. Shapiro, S. L., Springer : Berlin 1977, 83

5.11   Okamoto, H., Nakabayashi, T. and Tasumi, M. (1993) *Incoherent Time-Resolved Pump-Probe Raman Spectroscopy*, J. Phys. Chem. **97**, 9871

5.12   Okamoto, H., Nakabayashi, T. and Tasumi, M. ( ) *Time-Resolved Pump-Probe Raman Spectroscopy with Temporally Incoherent Light* .

5.13 Morita, N., Tokizaki, T. and Yajima, T. (1987) *Time delayed four-wave mixing using incoherent light for observation of ultrafast population relaxation*, J. Opt. Soc. Am. B **4**, 1269

5.14 Liu, J., Huang, S., Qin, W. and Yu, J. (1993) *Measurement of the picosecond population relaxation time of Cresyl Violet by time-delayed four-wave mixing with incoherent light*, Journal of Luminescence **54**, 319

5.15 Okamoto, H. (1993) *Ultrafast population relaxation by time-resolved degenerate four-wave mixing with incoherent light and analysis under breakdown of the two-level approximation*, J. Opt. Soc. Am. B **10**, 2353

5.16 Fujiwara, M. and Kuroda, R. (1985) *Measurement of ultrafast dephasing of Cresyl Fast Violet in cellulose by photon echoes with incoherent light*, J. Opt. Soc. Am. B **2**, 1634

5.17 Kobayashi, T., Hattori, T. and Kurokawa, K. (1987) *Femtosecond relaxation processes in nonlinear materials studied with incoherent light*, Revue Phys. Appl. **22**, 1773

5.18 Vardney, Z.V. (1993) *Ultrafast Spectroscopy of Conducting Polymers*, Journal of Molecular Structure **292**, 279

5.19 Kobayashi, T., Hattori, T., Terasaki, A. and Kurokawa, K. ( ) *Femtosecond studies of dephasing and phase conjugation with incoherent light*

5.20 Meech, S.R., Hoff, A.J. and Wiersma, D.A. (1985) *Evidence for a very early intermediate in bacterial photosynthesis . A photon-echo and hole burning study of the primary donor band in rhodopseudomonas sphaeroides*, Chem. Phys. Lett. **121**, 287

5.21 Tomita, M. and Matsuoka, M. (1986) *Ultrafast pump-probe measurement using intensity correlation of incoherent light*, J. Opt. Soc. Am. B **3**, 560

5.22 Ye, P. and Shen, Y.R. (1982) *Transient four-wave mixing and coherent transient optical phenomena*, Phys. Rev. A **25**, 2183

5.23 RELAXATION TIME OF DYES

5.24 Weiner, A.M., De Silvestri, S. and Ippen, E.P. (1985) *Three-pulse scattering for femtosecond dephasing studies: theory and experiment*, J. Opt. Soc. Am. B **2**, 654

5.25 Flytzanis, C. and Hutter, J. (1992) in *Contemporary Nonlinear Optics*, eds. , 297

5.26 Flytzanis, C., Hache, F., Klein, M. C., Ricard, D. and Roussignol, Ph. (1991) in *Progress in optics*, ed. Wolf, E., Elsvier Science Publishers, 321

5.27 Hache, F., Ricard, D., Flytzanis, C. and Kreibig, U. (1988) *The Optical Kerr Effect in Small Metal Particles and Metal Colloids : The Case of Gold*, Appl. Phys. A **47**, 347

5.28 Hache, F., Ricard, D. and Flytzanis, C. (1986) *Optical Nonlinearities of Small Metal Particles : Surface Mediated Resonance and Quantum Size Effects*, J. Opt. Soc. Am. B **3**, 1647

5.29 Hache, F., Ricard, D. and Flytzanis, C. (1989) *The Optical Kerr Effect in Small Metal Particles and Metal Doped Glasses: The Case of Gold*, in SPIE Vol. 1127 Nonlinear Optical materials II, ed. Grun, J-B, 115

CHAPTER 6

ULTRAFAST BEAM DEFLECTION METHOD FOR THE MEASUREMENT OF THE TRANSIENT REFRACTIVE INDEX OF MATERIALS

Numerous effects such as the optical Kerr effect,[1] interferometry [2, 3] and beam deflection methods,[4, 5] can be utilised for the measurement of the nonlinear index of refraction, n_2, in materials. The first two methods allow time resolution while the last, being a single beam method, only permits the determination of the magnitude of n_2 and provides no information on the dynamics of the nonlinear interaction. If, however, a second beam is used in an experiment that measures beam deflection or distortion, it is possible to actually resolve the interaction in time. Based on this idea. Albrecht et al [6] devised an ultrafast beam deflection technique for measuring the induced change of the refractive index of a nonlinear material that offers simplicity and sensitivity, as well as time resolution on a fs timescale.

The principle of the experiment is depicted in figure 6.1. A weak probe pulse is incident, normally, on a sample placed behind an aperture. At the same time an intense pump pulse is incident on the same point, at an angle α with respect to the probe. The aperture ensures a definite, nearly rectangular spatial intensity profile and an accurate overlapping of both beams at the entrance of the sample. The presence of the pump pulse induces a refractive index change in the sample which consequently results in the probe beam being deflected by an angle θ. The extent of the deflection is a measure of the induced index change and its decay, as a function of delay time between the pump and probe beams, gives information on the dynamics of the material. The deflection of the probe is measured by a diode array.
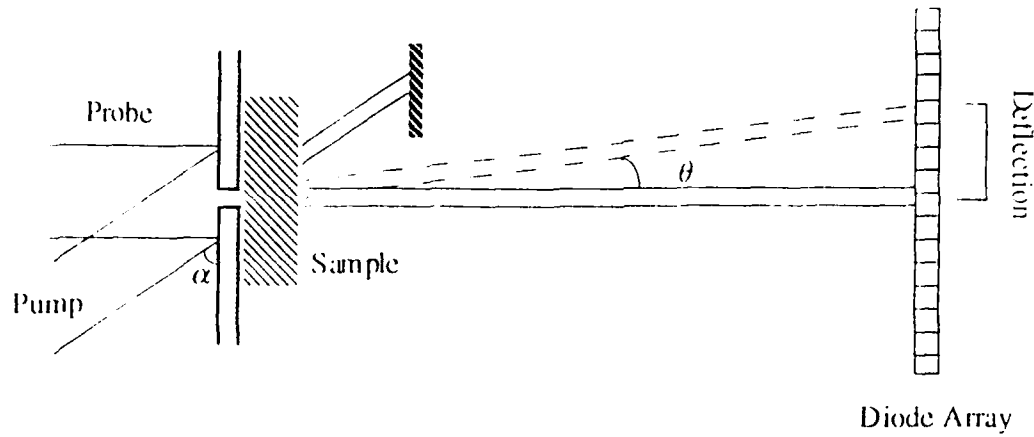
Figure 6.1 : Schematic diagram of the experimental set-up for measuring the transient nonlinear refractive index of materials.

The region of the sample irradiated by the pump has a resultant refractive index given by $n_0 + \Delta n$, where n_0 is the refractive index of the sample in the absence of the pump beam and Δn is the index change induced by it. The change in refractive index is related to the nonlinear index of refraction, n_2 through the equation:

$$\Delta n = n_2 I \tag{6.1}$$

where I is the intensity of the pump beam.

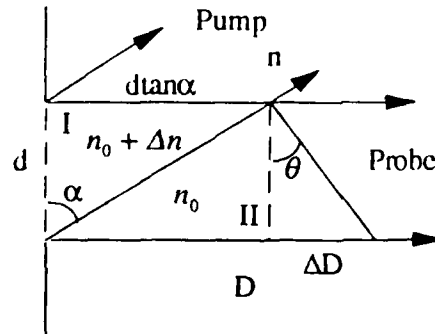It is possible to relate n_2 to the deflection of the probe beam by using Snells law.

Figure 6.2 : Geometrical construction showing the relationship between Δn and the deflection angle θ.

In region 1, the probe beam travels through a medium of refractive index given by $n_0 + \Delta n$ with a velocity $V = \dfrac{c}{n_0 + \Delta n}$. The total distance travelled is given by $d \tan \alpha$ and the time taken is, therefore, $t = \dfrac{d \tan \alpha}{c}(n_0 + \Delta n)$.

83

In region 2, the probe beam travels through a medium of refractive index n with a velocity $\frac{c}{n_o}$. In time t it travels a distance $\frac{d\tan\alpha}{n_o}\cdot(n_o + \Delta n)$.

From figure 2, thus, $\tan\theta = \frac{\Delta n}{n_o}\tan\alpha$. When $\theta \to 0$, $\tan\theta \to \sin\theta$, and hence we get:

$$\sin\theta = \frac{\Delta n}{n_o}\tan\alpha \qquad (6.2)$$

which is the same as the result obtained by Albrecht et al.[6]

The greater the deflection of the probe beam, the greater will be the resolution of the experiment. To achieve high deflection angles α is chosen to be close to 86° which results in an interaction length of ≈ 2mm. When using fs pulses it is very important to avoid having very long interaction lengths as this results in an increase in the pulse duration due to group velocity dispersion in the sample. For an interaction length of 2mm, group velocity dispersion is negligible. The diode array that records the deflection of the probe beam consists of pixels 25µm wide and is at a distance of ≈ 415mm from the aperture. Therefore a displacement of one pixel corresponds to a deflection angle of 6×10^{-5} radians.

The experiment was performed by measuring the deflection of the probe beam as a function of delay time between the pump and probe beams. Hence it is possible to determine, simultaneously, both the magnitude and the response time of the nonlinear refractive index. It is also possible to determine the sign of n_2 by comparing the deflection observed for water with that observed for the sample. The reason that the comparison was done with water is that it was the solvent used. If the beam through the sample is deflected less than it is for pure water then n_2 is negative, which is intuitively obvious. This was the case for all the gold colloids tested.

The laser system consisted of a CPM dye laser (λ = 616nm, pulse width = 75fs) followed by an Excimer-laser pumped amplifier cascade split by a beam splitter into a strong pump pulse and a weak probe pulse. The width of the aperture was 150µm and the diameter of the 2 beams was 400 µm. A polariser was placed in front of the probe beam, oriented at 45^0 to the plane of the pump polarisation. An analyser placed before the detector, thus made possible the separate measurement of the probe pulse components parallel and perpendicular to the pump pulse.

Figure 6.3 shows a typical result obtained. The sample is a 18nm gold colloid in de-ionised water. Also shown on the same graph is the deflection for water as a function of delay time. The polarisations of the pump and probe beams are parallel.
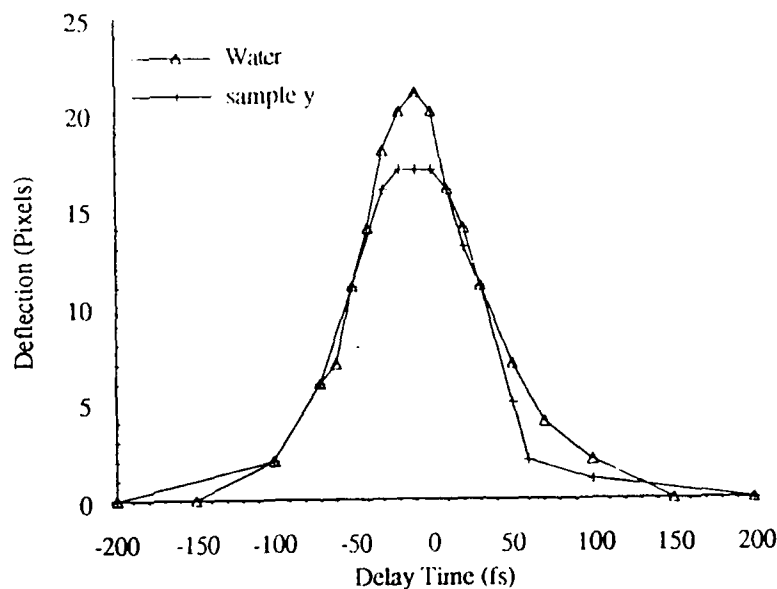

Figure 6.3 : Sample Y, Probe Beam Deflection Vs Delay time.

As is evident from the graph, at zero delay, the deflection for sample Y is 17 pixels while the deflection for pure water is 21 pixels. Taking the value of n_2 for water to be $3.8 \times 10^{-16} cm^2 / W$, we get, for the inclusions :

$$n_2 = -7.24 \times 10^{-17} cm^2 / W.$$

n_2 and $\chi^{(3)}$ are related through the formula :[7]

$$n_2 = \frac{3}{4} \frac{\chi^{(3)}}{n_0^2 \varepsilon_0 c} \qquad (6.3)$$

Using equation 6.3, therefore it is possible to obtain a value for $\chi^{(3)}$ for the samples measured. The results are tabulated in table 6.1.

Sample	Particle Size (Å)	Vol. Fraction of Particles	Abs. Coeff. $\alpha(cm^{-1})$	χ $(m\ V^{-2})$
M	392	2.54×10^{-5}	1.994	-3.97×10^{-23}
N2	395	7.05×10^{-6}	0.688	-5.10×10^{-23}
N1		1.20×10^{-6}	0.176	-1.70×10^{-23}
P2	52	2.48×10^{-5}	3.473	-9.27×10^{-23}
P1		7.13×10^{-6}	0.945	-3.40×10^{-23}
Q2	47	1.94×10^{-5}	2.588	-7.96×10^{-23}
Q1		2.78×10^{-6}	0.391	-3.40×10^{-23}
S3	185	1.02×10^{-5}	1.169	-3.96×10^{-23}
S2		6.20×10^{-6}	0.499	-5.10×10^{-23}
S1		2.48×10^{-6}	0.281	-1.70×10^{-23}
Y2	179	4.58×10^{-6}	0.375	-4.54×10^{-23}
Y1		2.43×10^{-6}	0.213	-2.27×10^{-23}

Table 6.1 : Experimental Results

Six different samples were measured, with each sample, except M, being measured at two or more concentrations. As was observed with previous experiments, again there is no relationship between $\chi^{(3)}$ and particle size. However $\chi^{(3)}$ is again found to be proportional to the square of the absorption coefficient. Figure 6.4 shows this result.
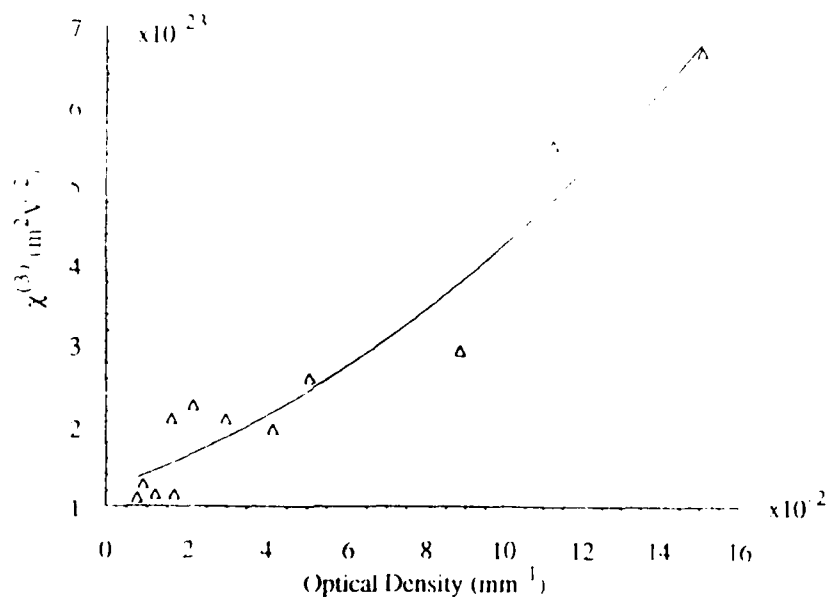

Figure 6.4 : $\chi^{(3)}$ Vs Absorption Coefficient.

As was explained earlier, in chapter 2, the nonlinearity associated with the actual gold particles is related to the effective nonlinearity of the solution through :

$$\chi_i^{(3)} = \frac{\chi^{(3)}}{p|f_1|^4}$$ (6.4)

Where $\chi_i^{(3)}$ is the third order susceptibility of the gold particles, p is their volume fraction and the factor f_1 is a local field factor. At the surface plasmon resonance frequency it is greater than unity and serves to enhance the effective nonlinearity of the solution significantly. Off resonance however, $f_1 < 1$ and $\chi^{(3)}$ is, in fact, diminished. This can be seen by comparing the results for $\chi^{(3)}$ at 616nm (this chapter)with those at 522 nm (Chapters 3 and 5).

The field enhancement factor is size dependent in that it depends on the width of the surface plasmon resonance band, which should in turn be proportional to the size of the inclusions. However, in all the colloids measured, there were no significant differences in the widths of the absorption bands, despite the disparity in sizes.

f_1 is determined using the equation :

$$f_1 = \frac{3(\varepsilon_d)}{\varepsilon_i + 2\varepsilon_d}$$ (6.5)

Where ε_d (real) is the dielectric constant of the solvent (dielectric matrix),

and ε_i (imaginary) is the dielectric constant of the gold particle.

At $\lambda = 616$nm, it turns out to be approximately 0.7, much the same for all the samples.

Using equation 6.4, therefore, $\chi_i^{(3)}$ can be determined. The results are tabulated in table 6.2.

Sample	Particle Size (Å)	$\chi'^{(3)}$ (m V⁻²)	$\chi''^{(3)}$ (m V⁻²)
M	392	-3.97×10^{-23}	-7.00×10^{-18}
N2	395	-5.10×10^{-23}	-3.16×10^{-17}
N1		-1.70×10^{-23}	-6.21×10^{-17}
P2	52	-9.27×10^{-23}	-1.62×10^{-17}
P1		-3.40×10^{-23}	-2.07×10^{-17}
Q2	47	-7.96×10^{-23}	-1.74×10^{-17}
Q1		-3.40×10^{-23}	-5.22×10^{-17}
S3	185	-3.96×10^{-23}	-1.52×10^{-17}
S2		-5.10×10^{-23}	-3.23×10^{-17}
S1		-1.70×10^{-23}	-2.68×10^{-17}
Y2	179	-4.54×10^{-23}	-3.84×10^{-17}
Y1		-2.27×10^{-23}	-3.61×10^{-17}

Table 6.2 : $\chi_r^{(3)}$ values for the different samples.

The values obtained for $\chi_r^{(3)}$ are about an order of magnitude lower than those obtained at resonance. ($\lambda = 522$nm). This is to be expected as the experiment only measures the real part of the effective susceptibility. In any case, the contribution of the absorptive effect (predominantly imaginary) should be significantly reduced at this wavelength.

The decay of the probe beam deflection as a function of delay time between the pump and probe beams yields information on the dynamics of the interaction. The resolution of the experiment is limited on the pulse width of the laser beam. If the response time of the nonlinearity is fast on the timescale of the pulse width, then the decay curve is equivalent to the autocorrelation profile of the beam. If, on the other hand, the nonlinearity responds much more slowly, then the deflection decays with a characteristic time dependent on the energy relaxation time, T_1 of the sample. In the case of most of the samples measured, it turns out that T_1 is in fact fast on the timescale of the pulse width which is 75 fs. This is evident by referring back to figure 6.3. Here, the only thing that we can do is put an upper limit of 75 fs on T_1. Two of the samples show a slightly different behaviour. They are the two smallest colloids P and Q of sizes of the order 50Å. In these two cases, the deflection decays on a time scale of about 600 fs. The decay profile for the two samples is shown in figure 6.5 :
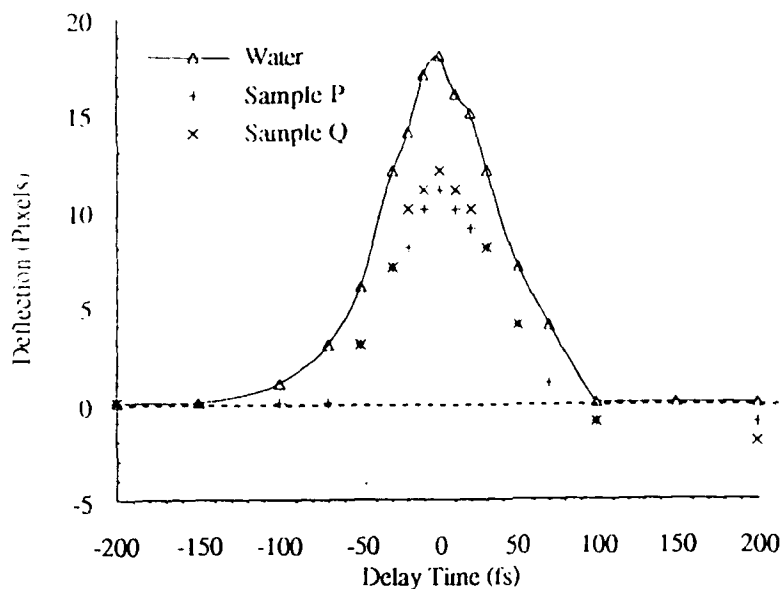
Figure 6.5 : Samples P and Q, Probe Beam Deflection Vs Delay Time.

The reason that these two samples behave differently to the rest is obviously related their small diameter. When the size of the colloidal particle goes below a particular threshold level, it starts to behave like a single molecule and molecular states come into being. Molecular states characteristically decay on a much slower timescale than electronic states. (????)

REFERENCES

6.1 Thomazeau, J., Etchepare, J., Grillon, G. and Migus, A. (1985) Opt. Lett. **10**, 223

6.2 Hattori, T., Okawa, H., Wada, T. and Sasabe, H. (1992) Opt. Lett. **17**, 1560

6.3 Tokunaga, E., Terasaki, A., Kobayashi, T. (1992) Opt. Lett. **17**, 1131

6.4 Sheik-bahae, M., Said, A. A. and van Stryland, E. W. (1989) *High Sensitivity, Single Beam n, Measurements*, Opt. Lett. **14**, 955

6.5 Sheik-bahae, M., Said, A. A., Wei, T. H., Hagan, D.J. and van Stryland, E. W. (1990) *Sensitive Measurement of Optical Nonlinearities using a Single Beam*, IEEE J. Quant. Elec. **26**, 760

6.6 Albrecht, H. S., Heist, P., Kleinschmidt, J. and Lap, D.V. (1993) *Ultrafast Beam-Deflection Method and its Application for measuring the Transient Refractive Index of Materials*, Appl. Phys. B **57**, 193

6.7 Butcher, P. N. and Cotter, D. (1990) in *The Elements of Nonlinear Optics*, Cambridge university Press, 306

CHAPTER 7

CONCLUSIONS

Experimental results, so far, have never shown such a size dependence. The reason being that the intraband contribution (above) in actual metal crystallites is not the sole polarisation mechanism. Two more mechanisms contribute there with quite different behaviour that dominates that of the intraband term. One mechanism is the interband term that arises from the electronic dipole transitions between the filled d band states and the empty confined ones in the s-p band, and gives a contribution that is negative imaginary but size independent as the d electrons are unaffected by the confinement.

The other mechanism is the hot electron contribution that results from the modification of the population of the electron states, the Fermi-Dirac distribution, caused by the elevation of their temperatures subsequent to the absorption of photons in the resonant process, but before the heat is released to the lattice of the crystallite; this leads to a contribution to $\chi^{(3)}$ that is positive imaginary and size independent.

From experiments performed so far, it seems that the dominant contribution to $\chi^{(3)}$ comes from the third mechanism and also that even the interband term dominates the intraband term.